# **Learning Generalizable Shape Completion with SIM(3) Equivariance**

Yuqing Wang<sup>1\*</sup> Zhaiyu Chen<sup>1,2\*</sup> Xiao Xiang Zhu<sup>1,2</sup>

<sup>1</sup>Technical University of Munich 
<sup>2</sup>Munich Center for Machine Learning

#### **Abstract**

3D shape completion methods typically assume scans are pre-aligned to a canonical frame. This leaks pose and scale cues that networks may exploit to memorize absolute positions rather than inferring intrinsic geometry. When such alignment is absent in real data, performance collapses. We argue that robust generalization demands architectural equivariance to the similarity group, SIM(3), so the model remains agnostic to pose and scale. Following this principle, we introduce the first SIM(3)-equivariant shape completion network, whose modular layers successively canonicalize features, reason over similarity-invariant geometry, and restore the original frame. Under a de-biased evaluation protocol that removes the hidden cues, our model outperforms both equivariant and augmentation baselines on the PCN benchmark. It also sets new cross-domain records on real driving and indoor scans, lowering minimal matching distance on KITTI by 17% and Chamfer distance  $\ell 1$  on OmniObject3D by 14\%. Perhaps surprisingly, ours under the stricter protocol still outperforms competitors under their biased settings. These results establish full SIM(3) equivariance as an effective route to truly generalizable shape completion. Project page: https://sime-completion.github.io.

### 1 Introduction

3D scans are often riddled with gaps due to occlusions and limited sensor coverage. Completing the missing geometry lets robots plan stable grasps, autonomous vehicles reason about hidden traffic, and curators digitize heritage artifacts without repeated scanning [1, 2, 3, 4]. However, most shape completion methods [5, 6, 7, 8] are developed on curated benchmarks where every scan is prealigned to a canonical frame with a fixed pose and scale relative to ground truth. These leaked cues inadvertently bias learning: instead of inferring intrinsic geometry, neural networks tend to memorize where shapes reside in that frame, leading to inflated performance that collapses once the alignment is removed in practice [9, 10]. The resulting gap between benchmark success and real-world reliability highlights the challenge of exploiting geometry without inheriting extrinsic transforms that convey it.

Data augmentation mitigates this alignment bias by randomizing transforms during training to approximate inference-time invariance, but it entangles those transforms with underlying geometry and leaves the core ambiguity unresolved. Architectural equivariance, by contrast, aims to ensure that applying a transform to the input induces the same transform in the prediction, thereby isolating geometry from transforms and sharpening learned representations [11, 12]. However, existing equivariant methods still struggle to enforce this separation. SO(3)-equivariant shape completion [13, 14] typically normalizes inputs using ground-truth centroids and scales, while SE(3)-equivariant variants [10, 15, 16] still rely on ground-truth scale to canonicalize scans. Relying on such privileged information effectively reduces these models to explicit canonicalization (Fig. 1), undermining the true purpose of equivariance. To our knowledge, no existing architecture fully eliminates alignment bias, as all still require some ground-truth alignment that is unavailable in practice.

<sup>\*</sup> Equal contribution. Corresponding author: zhaiyu.chen@tum.de.

We argue that true generalization hinges on handling arbitrary similarity transforms, SIM(3), including rotation, translation, and scaling. To this end, we present the first shape completion architecture whose modules are SIM(3)-equivariant by design. During training, the network learns representations agnostic to pose and scale; at test time, any similarity transform applied to the input induces identical changes in the prediction (Fig. 1). To recover the completed shape in the sensor frame, we introduce a lightweight restoration path that re-injects the transform information progressively. By disentangling

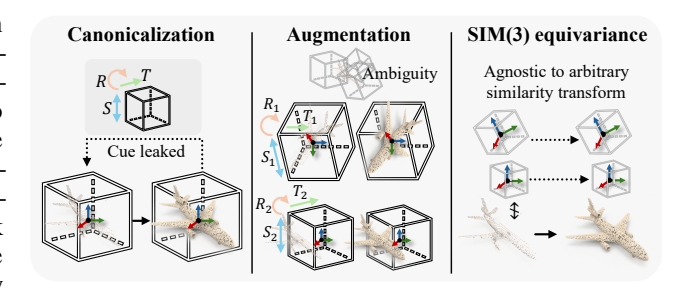


Figure 1: Three paradigms for shape completion. Explicit canonicalization, including SO(3)- and SE(3)-equivariant variants, leak pose and scale cues and fail on non-canonical inputs. Data augmentation mitigates the alignment bias but incurs ambiguity. We present a SIM(3)-equivariant approach that generalizes to arbitrary similarity transforms.

intrinsic geometry from extrinsic transforms, our model trained on synthetic data transfers directly to real scans under a fair, de-biased evaluation protocol. In summary, our contributions include:

- 1. **Problem identification.** We reveal pose and scale bias in existing shape completion methods, and identify SIM(3) equivariance as a prerequisite for reliable, in-the-wild generalization.
- 2. **Generalizable framework.** We develop the *first* fully SIM(3)-equivariant network for shape completion. It integrates feature canonicalization, similarity-invariant geometric reasoning, and a transform restoration path into a modular design, generalizing from synthetic to real scans.
- 3. **Protocol and resources.** We establish a rigorous evaluation protocol that eliminates hidden pose and scale bias, release code for reproducibility, and provide thorough analyses that pinpoint where equivariance delivers its gains. Under this protocol our method sets a new state of the art.

#### 2 Related Work

**Equivariant 3D representations.** Equivariant neural networks learn features that transform consistently under input symmetry operations. Grounded in group theory and representation learning [11, 17, 18, 19, 20, 21, 22, 23, 24, 25, 26, 27], 3D equivariant models have been developed to handle variability in data transforms. One approach employs group convolution [28, 29, 30] to encode symmetry, but these methods often remain bound to specific architectures and lack generality. Another leverages tensor algebra with spherical harmonics as irreducible representations to achieve equivariance [12, 31]. Vector neurons (VN) [32] replaced high-order tensors with structured 3D vectors, providing a modular SO(3)-equivariant alternative. Subsequent extensions integrated attention mechanisms [33] and translation equivariance [34], yet most VN-based networks remain relatively shallow, which limits their applicability to complex 3D tasks. Nonetheless, both paradigms have driven advances in 6-DoF pose estimation [35, 36, 37], point cloud registration [38, 39], robotic manipulation [40, 41], and 3D reconstruction [42, 43, 44], among others [45, 46]. However, most methods are confined to SO(3) or SE(3) equivariance and require centering or scale normalization. Both assumptions break down in real-world scenarios without ground truths. Although SIM(3)equivariance can overcome these limitations, existing efforts [40, 41, 46] remain sparse, depend on near-complete inputs, and struggle on partial observations. We close this gap with a fully SIM(3)equivariant Transformer architecture.

**3D shape completion.** Early methods represented geometry in voxels and applied 3D CNNs [5, 47, 48, 49], but cubic complexity limited resolution. The use of symmetric functions for permutation invariance [50] led to the development of shape completion networks that directly consume 3D points [51, 52]. More recently, Transformers [53] have recast shape completion as set-to-set translation [6], and now lead the field [7, 8, 54, 55, 56, 57]. Almost all prior work, however, presumes that inputs are pre-aligned to the training frame, letting pose and scale cues leak into models and collapse performance on raw scans without special adaptation [9, 58]. Existing remedies follow two paradigms. Data augmentation randomizes transforms during training, but entangles extrinsic transforms with intrinsic geometry and incurs ambiguity at test time. Equivariance-based methods

either estimate a canonical pose prior to completion [15, 16] or replace standard layers with equivariant variants [10, 13]. The former relies on a fragile pose estimator that misaligns under partial observations and propagates errors for the downstream completion. The latter often loses fine-grained details and underperforms Transformer models with data augmentation [13]. A recent anchor-point scheme extends equivariance to SE(3) [10], but its dependence on brittle anchor selection hampers performance and still falls behind augmented baselines. Moreover, all these methods still rely on ground-truth bounding boxes to cancel scale variance, re-introducing the very cues they aim to discard. In contrast, we integrate full SIM(3) equivariance into every layer, inherently agnostic to arbitrary pose and scale, delivering the first shape completion method that truly generalizes to completely unaligned real-world scans.

# 3 Method

#### 3.1 Preliminaries

**Formulation.** Shape completion,  $f_{\theta} \colon \mathbf{x} \to \hat{\mathbf{y}}$ , takes a partial observation  $\mathbf{x} = \{x_i \in \mathbb{R}^3\}_{i=1}^{N_{\text{in}}}$  (e.g., a point set) and aims to reconstruct a set  $\hat{\mathbf{y}} = \{\hat{y}_i \in \mathbb{R}^3\}_{i=1}^{N_{\text{out}}}$  representing the completed shape, both expressed in the original sensor frame. Due to varying capture conditions,  $\mathbf{x}$  and its ground truth  $\mathbf{y}$  may undergo a shared unknown similarity transform  $g = (s, R, t) \in \text{SIM}(3)$ :

$$\mathbf{x}' := g \cdot \mathbf{x} = sR\mathbf{x} + t, \quad \mathbf{y}' := g \cdot \mathbf{y} = sR\mathbf{y} + t, \quad s \in \mathbb{R}_+, \ R \in SO(3), \ t \in \mathbb{R}^3, \quad (1)$$

where  $\mathbf{x}'$  and  $\mathbf{y}'$  are transformed representations of the same object. Although the transform g alters coordinates, the intrinsic geometry remains invariant. To guarantee consistent predictions under any similarity transform, we enforce  $\mathrm{SIM}(3)$  equivariance in  $f_{\theta}$ . Paired with a permutation-invariant loss  $\mathcal{L}(f_{\theta}(\mathbf{x}), \mathbf{y})$  (e.g., Chamfer distance), we solve the constrained optimization problem:

$$\min_{\theta} \mathcal{L}(f_{\theta}(\mathbf{x}), \mathbf{y}) \quad \text{s.t.} \quad f_{\theta}(g \cdot \mathbf{x}) = g \cdot f_{\theta}(\mathbf{x}) \ \forall g \in \text{SIM}(3).$$
 (2)

**Vector neurons.** To enforce the equivariance constraint in Eq. (2), we build on the vector neuron (VN) framework [32], which replaces scalar neurons with 3D vector ones. At layer l, we organize  $D^l$  vector channels into M vector features:

$$\mathcal{V}^l = \{ \mathbf{V}_i^l \}_{i=1}^M, \quad \mathbf{V}_i^l \in \mathbb{R}^{D^l \times 3}. \tag{3}$$

The VN framework defines linear, nonlinear, and pooling operations on these vector neurons to preserve symmetry under the SO(3) group action. We adapt VN representations and integrate these operations as building blocks into our SIM(3)-equivariant architecture. For simplicity, we omit the layer index l in the following unless cross-layer operations are involved. See Appendix  $\mathbb{C}$  for details.

**Challenges.** We decompose the overall objective in Eq. (2) into three complementary requirements, separating geometric reasoning from transform alignment:

$$\min_{\theta} \begin{cases}
\mathcal{L}(g^{\star} \cdot f_{\theta}(\mathbf{x}), \mathbf{y}) & \text{Req. (1) geometric reasoning} \\
\|g^{\star} - \mathbf{I}\| & \text{Req. (3) transform alignment}
\end{cases} \text{ s.t. } \underbrace{f_{\theta}(g \cdot \mathbf{x}) = g \cdot f_{\theta}(\mathbf{x})}_{\text{Req. (2) equivariance}}. (4)$$

Here  $g^*$  denotes the optimal alignment between the prediction and the ground truth, such that  $\mathcal{L}(g^* \cdot f_{\theta}(\mathbf{x}), \mathbf{y})$  measures geometric discrepancy independent of pose and scale. In this formulation:

- **Req. (1) Geometric reasoning.** The network must infer the complete geometry of missing regions, even when x are sparsely and heterogeneously sampled. This demands strong structural priors and fine-grained feature extraction that shallow architectures cannot achieve.
- **Req. (2) Equivariance.** The model must respect SIM(3) symmetry, which needs to be enforced throughout, because any single layer that is not equivariant will break global equivariance. Thus, each operator must be redesigned to commute with the group actions.
- **Req. (3)** Transform alignment. The completed shape  $f_{\theta}(\mathbf{x})$  must be presented in the sensor frame so that no further alignment is required for downstream tasks. Equivalently,  $g^*$  should remain close to the identity transform I under any reasonable metric  $\|\cdot\|$ . This requires propagating pose and scale information throughout the network to preserve the original frame.

The next section details how each component of our architecture satisfies these requirements.

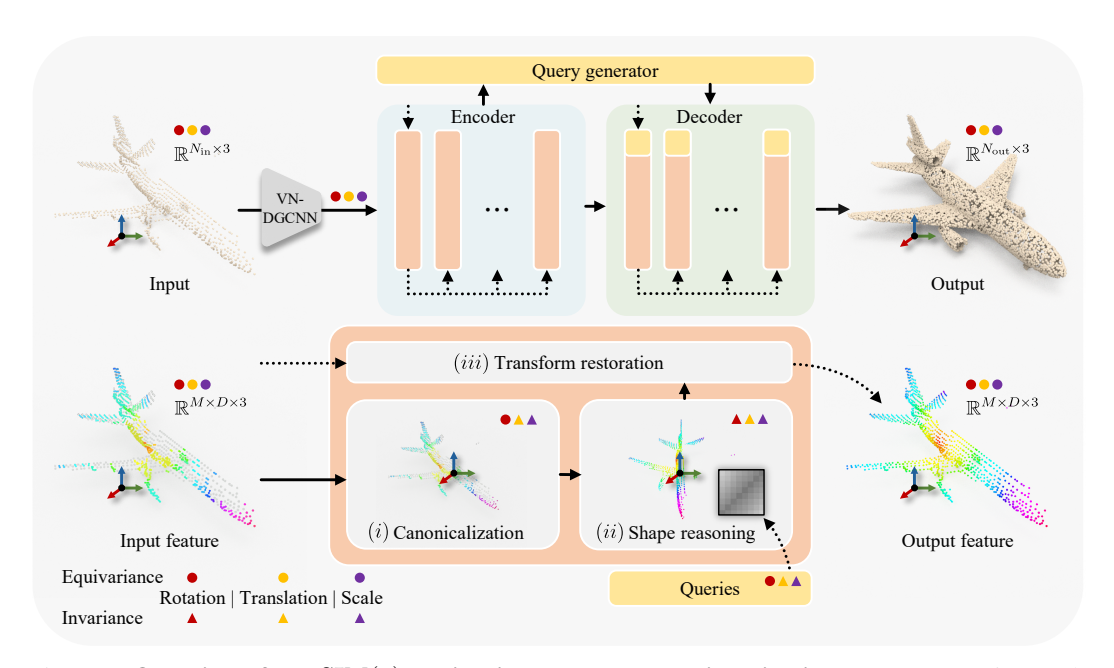


Figure 2: Overview of our SIM(3)-equivariant shape completion pipeline. We extract point patch features with VN-DGCNN [32] and feed them into a Transformer encoder-decoder. Within each layer module, we (i) canonicalize features to be translation- and scale-invariant, (ii) reason intrinsic geometry via SIM(3)-invariant attention, and (iii) restore the original transform. This guarantees that both intermediate features and the reconstructed shape adhere to SIM(3) transforms.

# 3.2 SIM(3)-equivariant shape completion

We progressively address the three challenges in Eq. (4) via  $L \operatorname{SIM}(3)$ -equivariant blocks, which enforce the equivariance constraint as in Req. (2) by design:

$$\mathcal{B}^l = \mathcal{R}^l \circ \mathcal{A}^l \circ \mathcal{C}^l, \quad f_{\theta}(x) = \mathcal{B}^L \circ \cdots \circ \mathcal{B}^1(x). \tag{5}$$

Each block  $\mathcal{B}^l$  comprises three sequential stages (Fig. 2): (i) feature canonicalization  $\mathcal{C}^l$  produces translation- and scale-invariant feature vectors; (ii) similarity-invariant shape reasoning  $\mathcal{A}^l$  optimizes Req. (1); and (iii) pose and scale are restored via  $\mathcal{R}^l$  to satisfy the transform-alignment objective in Req. (3). By stacking these blocks and end-to-end optimizing Eq. (4), the network iteratively refines its prediction and converges to the completed shape expressed in the input frame.

Canonicalization. Robust geometric reasoning requires removing transform variance embedded in the feature representation. As shown in Fig. 3, we extend layer normalization [33, 59, 60] to explicitly factor out global translation and scale from shape features. Specifically, let  $ar{\mathbf{V}}_i \in \mathbb{R}^3$  denote the channelwise mean of the latent vectors. We first subtract this mean from each  $V_i$ to eliminate translation, then normalize the centered vector to remove scale variation, followed by a vanilla layer normalization applied to the row-wise norm  $\left\|\mathbf{V}_i - \bar{\mathbf{V}}_i \right\|_2 \in \mathbb{R}^{D \times 1}$  to stabilize training without altering the direction of the vector neurons, thus preserving rotational consistency. Formally, the ex-

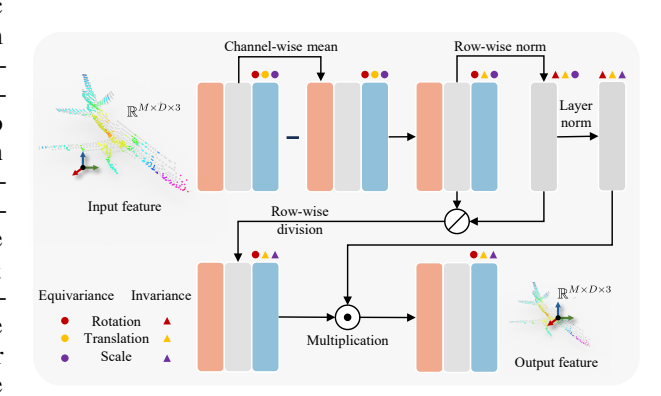


Figure 3: **Layer normalization.** We extend standard layer normalization [59] to producing translation- and scale-invariant features and preserving rotation equivariance.

tended layer normalization is defined as:

$$C^{l}: \quad \mathbf{V'}_{i} = \operatorname{layernorm}(\|\mathbf{V}_{i} - \bar{\mathbf{V}}_{i}\|_{2}) \frac{\mathbf{V}_{i} - \bar{\mathbf{V}}_{i}}{\|\mathbf{V}_{i} - \bar{\mathbf{V}}_{i}\|_{2}}. \tag{6}$$

This procedure canonicalizes features to an implicitly defined canonical feature frame.

**Shape reasoning.** In the scale- and translation-invariant canonical feature frame after  $\mathcal{C}^l$ , we perform similarity-invariant shape reasoning via the rotation-invariant attention weights **A** from VN-Transformer [33], ensuring no residual rotational bias. Since attention is invariant under any  $g \in \text{SIM}(3)$ , the local form of the objective in Req. (1), for each shape reasoning layer, reduces to:

$$\mathcal{A}^{l}: \min_{\theta_{A}} \mathcal{L}(f_{\theta_{A}}(\mathbf{A}(\mathbf{x})), \mathbf{y}), \tag{7}$$

where 
$$a_{ij} = \operatorname{softmax}_{j} \left( \frac{1}{\sqrt{3D}} \langle \mathbf{W}_{Q} \mathbf{V}'_{i}, \mathbf{W}_{K} \mathbf{V}'_{j} \rangle_{F} \right), \quad a_{ij} \in \mathbf{A}(\mathbf{x}).$$
 (8)

Here, the query and key projections  $\mathbf{W}_Q$ ,  $\mathbf{W}_K \in \mathbb{R}^{D \times D}$ , included in the model parameters  $\theta$ , define how shape features interact. The Frobenius inner product  $\langle \cdot \rangle_F$  is invariant to joint rotation of  $\mathbf{V}'_i$  and  $\mathbf{V}'_j$ , making the attention weights depend solely on their relative geometry. The attention weights satisfy  $\mathbf{A}(g \cdot \mathbf{x}) = \mathbf{A}(\mathbf{x})$  for any  $g \in \mathrm{SIM}(3)$ , which decouples intrinsic shape features from transforms.

**Transform restoration.** SIM(3) equivariance alone does not guarantee that the shape reasoning output is aligned with the original sensor frame, as it preserves only relative pose and scale. The final challenge is to recover this absolute alignment, as required in Req. (3). To achieve this, we introduce a transform restoration path to propagate input pose and scale via residual connections (Fig. 2). After each SIM(3)-invariant shape reasoning step, the restoration path reinjects translation and scale to recover spatial grounding. Rotation is implicitly preserved through the attention output  $\mathbf{Z}_i = \sum_j a_{ij} \mathbf{W}_{\mathbf{V}} \mathbf{V}'_j$ , where  $\mathbf{W}_{\mathbf{V}}$  is the value projection weight. Translation and scale are injected in accordance with their group actions via addition and multiplication, respectively:

$$\mathcal{R}^l: \quad \mathbf{V}^{l+1} = \mathbf{V}^l + \Phi(\mu^l \mathbf{Z}), \tag{9}$$

where  $\mu^l = \mathbb{E}_{D^l} \left\| \mathbb{E}_i(\mathbf{V}_i^l - \bar{\mathbf{V}}_i^l) \right\|_2$  is a global scale statistic computed from the average norm of centered input features, and  $\Phi$  is a VN linear layer that fuses spatial and geometric features to guide alignment. By restoring translation and scale at each stage, we reestablish full SIM(3) equivariance at the module output (see Appendix C for the proof), ensuring consistent spatial grounding across layers, as shown in Fig. 4.

### 3.3 Network architecture

We build on the AdaPoinTr [7] backbone, which features a coarse-to-fine shape completion scheme. We replace the original DGCNN with VN-DGCNN [32] for local geometric feature extraction while retaining SIM(3) equivariance, and replace every Transformer layer with our SIM(3)-equivariant module introduced in Sec. 3.2. Key components, such as the query generator and the reconstruction head, are likewise implemented to be equivariant or invariant when appropriate. The network takes a partial input point cloud with 2,048  $(N_{\rm in})$  points and predicts a complete shape of 16,384 ( $N_{\rm out}$ ) points. Aside from these changes, we retain AdaPoinTr's network depth, loss function, and training settings to

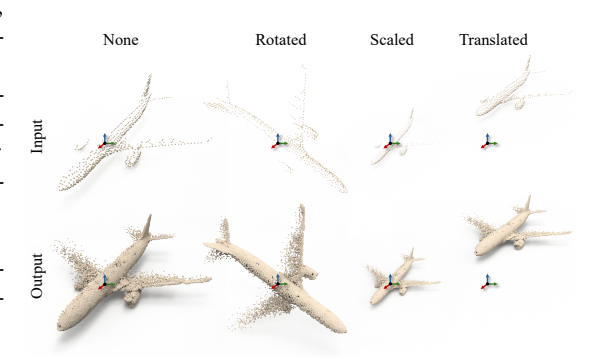


Figure 4: SIM(3) **equivariance.** Our outputs follow arbitrary similarity transforms applied to inputs.

ensure a fair comparison. Fig. 2 illustrates the architecture. Further architecture and implementation details are provided in Appendix C and D.

# 4 Experiments

# 4.1 Experimental setup

**Datasets and baselines.** We first evaluate on the PCN benchmark [51], which comprises eight categories from ShapeNet [61] with paired partial and complete point clouds. To assess cross-domain transferability, we directly apply PCN-trained models, without further normalization, to real-world scans from KITTI [62] and OmniObject3D [63]. We compare against leading non-equivariant shape completion methods, namely PoinTr [6], SeedFormer [54], SnowflakeNet [64], AnchorFormer [8], and AdaPoinTr [7], each trained with SIM(3) augmentations for fairness. Because no prior model offers full SIM(3) equivariance, we resort to including the SO(3)-equivariant EquivPCN [13] and the SE(3)-equivariant SCARP [15] and ESCAPE [10] as baselines.

**Evaluation protocol.** For our model, which requires no training-time augmentation, we adopt the train/test setting of I/SIM(3) where I denotes the identity transform. Each baseline is first evaluated under the group it was designed for (*i.e.*, I/SO(3) for EquivPCN [13], I/SE(3) for ESCAPE [10], and SE(3)/SE(3) for SCARP [15]) to reveal their upper-bound performance when pose/scale cues are still partly available. We then report their performance under SIM(3)/SIM(3) with additional data augmentation. On PCN, rotations are sampled uniformly from SO(3), while each partial input is *itself* centered and scaled to the unit sphere. This prevents cue leakage from ground truths and realistically simulates real-world inputs that models actually have access to. On KITTI and OmniObject3D, we transfer our model without any cue leakage, while competing equivariant methods receive canonicalized inputs via ground-truth alignment; otherwise, they fail completely. For PCN and OmniObject3D, we report Chamfer distance  $\ell_1$  (CD- $\ell_1$ , scaled by 10³) and F-score@1% (F1). For experiments on KITTI, we follow prior practices [6, 7, 8, 54] and report the Fidelity and Minimal Matching Distance (MMD) metrics. All metrics are computed in the common canonical frame with unit scale for direct comparison. We refer to our method as **SIMECO** in all comparisons.

#### 4.2 De-biased benchmark evaluation

Against data augmentation. Table 1 compares our SIM(3)-equivariant model against leading non-equivariant networks trained with augmentation. Our method achieves the *lowest* average  $CD-\ell_1$  and the *highest* F1 score, outperforming AdaPoinTr by 10% and 8%, respectively. It yields the best score in every category, with consistent error reductions across the board. Qualitative results in Fig. 5 show that our completions faithfully recover fine geometric details such as sharp airplane wings, slender lamp stems, and thin table legs, whereas the augmentation-based baseline produces blurrier or distorted shapes. Notably, AdaPoinTr without augmentation collapses under the de-biased protocol. These results confirm the superiority of our architectural equivariance over heavy data augmentation.

Table 1: **Evaluation on PCN.** We compare methods supporting only SO(3) (top) and SE(3) (middle), and those with SIM(3) augmentation (bottom). "Transform" indicate train/test settings. Our model outperforms competitors limited to partial transform groups and those with data augmentation.  $CD-\ell_1$  values are scaled by a factor of 1000. **Bold** numbers indicate the best SIM(3) results.

Method	Transform	Airpl.	Cab.	Car	Chair	Lamp	Sofa	Table	Wat.	$CD-\ell_1\downarrow$	F1 ↑
EquivPCN [13] AdaPoinTr [7]	I/SO(3) SO(3)/SO(3)	8.38 5.76	13.74 11.27	11.81 9.63	14.31 9.61	12.50 6.71	15.68 11.53	12.86 8.15	11.02 7.81	12.54 8.81	0.569 0.693
SCARP [15] ESCAPE [10] AdaPoinTr [7]	SE(3)/SE(3) I/SE(3) SE(3)/SE(3)	10.05 8.13 6.16	40.82 13.18 12.56	23.02 10.43 10.48	22.92 10.62 9.77	29.17 8.07 7.10	62.51 13.74 12.36	57.82 9.35 8.34	37.59 9.81 8.57	35.49 10.41 9.42	0.223 0.650 0.685
			Evaluatio	n under d	e-biased p	rotocol					
AdaPoinTr [7] EquivPCN [13] ESCAPE [10] PoinTr [6] SeedFormer [54] Snowflake [64] AnchorFormer [8] ODGNet [56] AdaPoinTr [7] SIMECO (ours)	I/SIM(3) SIM(3)/SIM(3) SIM(3)/SIM(3) SIM(3)/SIM(3) SIM(3)/SIM(3) SIM(3)/SIM(3) SIM(3)/SIM(3) SIM(3)/SIM(3) SIM(3)/SIM(3) SIM(3)/SIM(3) IM(3)/SIM(3) ISIM(3)/SIM(3)	31.93 9.10 12.59 10.18 8.42 7.99 7.77 6.16 6.46 <b>6.02</b>	78.90 14.60 22.54 17.97 17.32 15.59 13.61 11.60 12.17 10.75	63.51 13.09 18.63 15.61 15.08 13.81 12.13 11.15 10.51 <b>9.27</b>	60.56 15.74 15.86 16.94 12.10 11.89 12.71 10.13 10.29 <b>9.25</b>	61.47 13.74 12.68 13.39 8.25 8.58 9.16 6.81 7.59 <b>6.66</b>	70.77 16.42 24.38 16.80 17.19 15.66 14.26 13.12 12.26 11.16	71.94 14.74 14.17 17.75 11.38 10.59 10.95 9.48 8.90 <b>7.82</b>	42.74 11.74 14.48 12.18 9.62 9.72 9.35 8.19 8.14 7.77	60.23 13.65 16.88 15.10 12.42 11.73 11.24 9.58 9.54 <b>8.59</b>	0.206 0.523 0.515 0.434 0.616 0.621 0.599 0.659 0.661 <b>0.714</b>

Against equivariant networks. Table 1 benchmarks our method against other SO(3)- and SE(3)-equivariant networks, each evaluated under its native transform group. In contrast, by tackling the full SIM(3) group, we address a substantially harder setting. Despite this, our model reduces average CD- $\ell_1$  from 10.41 to 8.59 (-17%) and raises F1 from 0.650 to 0.714 (+10%) relative to ESCAPE, which uses the same AdaPoinTr backbone. EquivPCN (SO(3)) and SCARP (SE(3)) lag even further, confirming that full SIM(3) equivariance enables learning more intrinsic shape representations. Moreover, neither EquivPCN nor ESCAPE can outperform augmentation-based baselines in their respective groups. And training ESCAPE and EquivPCN with SIM(3) augmentation degrades their performance, highlighting that equivariance not built into the architecture is hard to acquire through augmentation alone. Figs 5 and 6 respectively demonstrate that our model preserves fine details and delivers consistent outputs under various pose and scale perturbations.

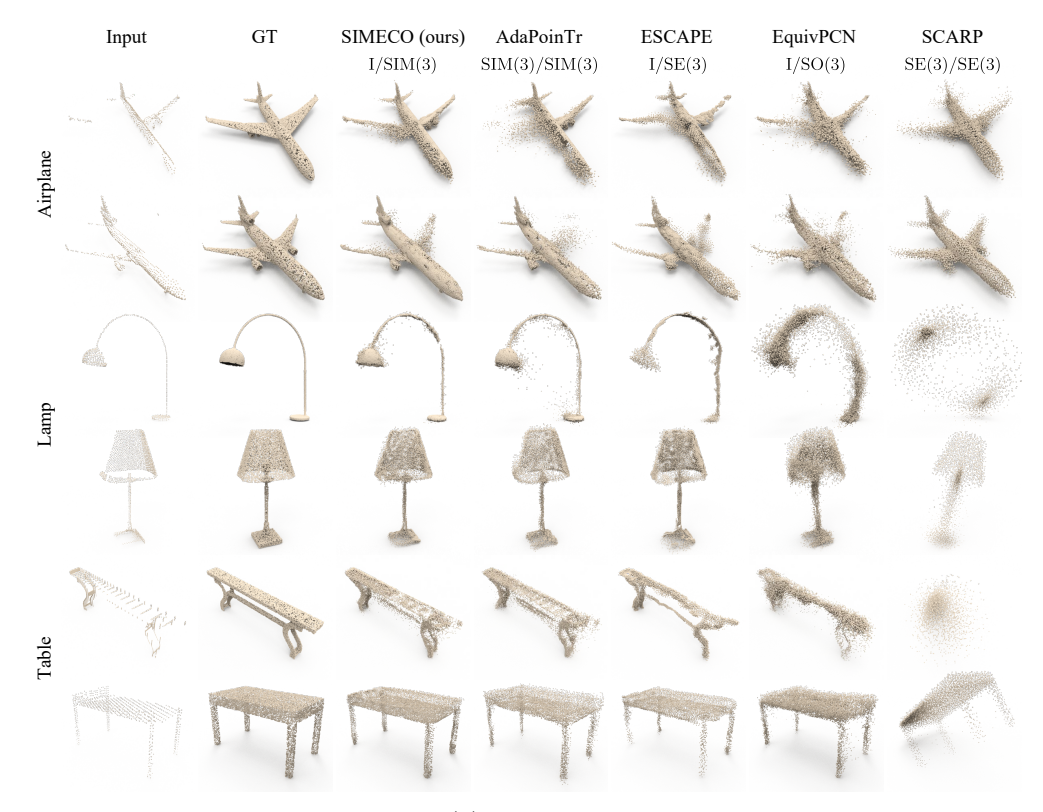


Figure 5: Comparison on PCN. Our SIM(3)-equivariant model outperforms other equivariant methods restricted to SO(3) and SE(3) and non-equivariant baseline trained with SIM(3) augmentation.

#### 4.3 Cross-domain generalization

Unseen driving scans (KITTI). Table 2 presents cross-domain performance on KITTI using models trained solely on synthetic, canonicalized PCN data. Even under full SIM(3) variation, our model reduces MMD from 6.47 to 5.35 (-17%) compared to the strongest non-equivariant baseline and cuts ESCAPE's Fidelity error from 1.81 to 0.56 (-69%). EquivPCN achieves even lower MMD, but only under its native SO(3) setting. Crucially, all competing methods, apart from those using data augmentation, rely on ground-truth bounding boxes to normalize KITTI inputs. SO(3) models use them for translation and scale normalization; SE(3) models use them for scale. This requirement leaks information and is impractical in real deployments. By contrast, our fully SIM(3)-equivariant architecture requires *no* external normalization. In Fig. 7, our model recovers car wheels and indoor details more faithfully, while AdaPoinTr with augmentation produces oversmoothed outputs.

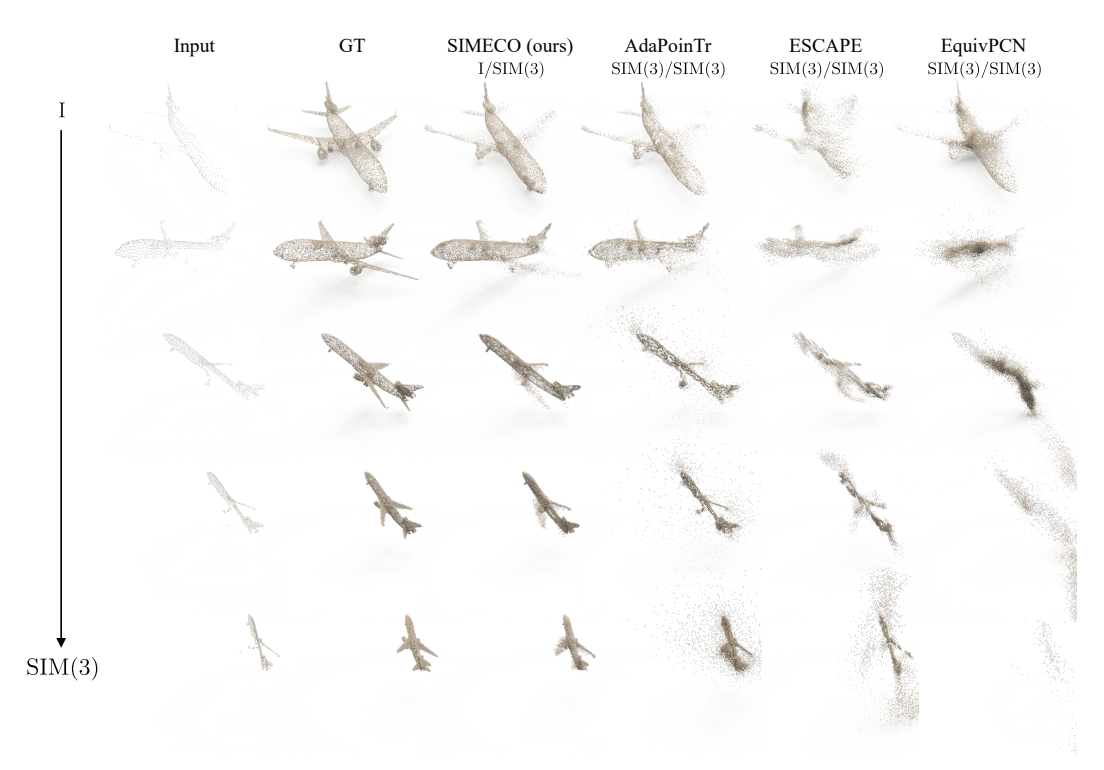


Figure 6: **Robustness to pose and scale perturbations.** Under larger pose and scale changes, our SIM(3)-equivariant model maintains completion quality, whereas competing methods degrade.

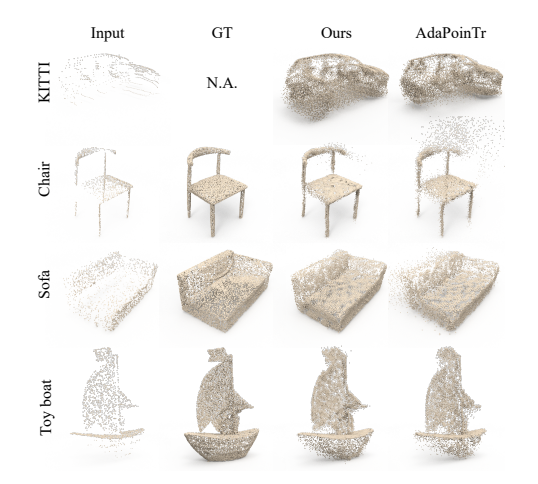


Figure 7: Cross-domain generalization to real scans. Our PCN-trained model completes driving (KITTI) and indoor (OmniObject3D) scans, with more details than the augmented baseline.



Figure 8: **Feature consistency.** Despite significant SIM(3) variations, feature maps from the PCN sample (outlined) and OmniObject3D scans exhibit matching structural patterns.

Unseen indoor scans (OmniObject3D). Table 3 presents cross-domain results on the diverse OmniObject3D benchmark. Our model achieves the *lowest* average  $CD-\ell_1$  and *highest* F1. Compared to the top non-equivariant baseline, we reduce  $CD-\ell_1$  by 14% and increase F1 by 5%. Relative to the SE(3)-equivariant ESCAPE, we achieve a 17% reduction in  $CD-\ell_1$ . These gains hold across all seven categories, with particularly notable improvements on *Cabinet* (14.69 *vs.* 17.15) and *Lamp* (11.07 *vs.* 14.03). Aside from augmentation-based methods, ours is the *only* 

Table 2: **Cross-domain performance on KITTI.** All methods are trained on PCN Cars.

Method	Transform	Fidelity $\downarrow$	$\mathrm{MMD}\downarrow$
EquivPCN [13]	I/SO(3)	0.413	3.293
SCARP [15]	SE(3)/SE(3)	2.733	10.020
ESCAPE [10]	I/SE(3)	1.810	5.930
PoinTr [6]	SIM(3)/SIM(3)	<b>0.000</b>	6.929
AdaPoinTr [7]	SIM(3)/SIM(3)	0.537	6.468
SIMECO (ours)	I/SIM(3)	0.558	<b>5.353</b>

model that generalizes without bounding-box normalization. Fig. 7 shows that our completions better preserve intricate geometric details.

Table 3: Cross-domain performance on OmniObject3D. Our model outperforms SO(3)- and SE(3)-equivariant methods and non-equivariant baselines trained with SIM(3) augmentation.

Method	Transform   Airpl.	Cab.	Car	Chair	Lamp	Sofa	Wat. $CD-\ell_1$	, F1↑
EquivPCN [13]	I/SO(3)   12.05	16.06	13.91	13.68	16.84	13.47	12.67   14.10	0.543
SCARP [15]	SE(3)/SE(3)   37.40	56.64	44.79	45.99	70.24	38.66	59.50   50.40	
ESCAPE [10]	I/SE(3)   9.89	15.79	11.87	7.78	19.49	11.12	10.41   12.34	
PoinTr [6]	SIM(3)/SIM(3)   12.11	26.40	18.98	12.48	25.38	16.83	14.81 18.14	0.664
AdaPoinTr [7]	SIM(3)/SIM(3)   11.48	17.15	12.10	7.44	14.03	10.73	10.38 11.90	
SIMECO (ours)	I/SIM(3)   <b>11.20</b>	<b>14.69</b>	<b>10.10</b>	<b>6.44</b>	<b>11.07</b>	<b>9.11</b>	<b>9.12 10.2</b> 3	

**Feature visualization.** Fig. 8 compares feature maps for a PCN sample alongside those from several OmniObject3D scans under different SIM(3) transforms. Despite large variations in pose and scale, the feature maps share strikingly similar structures, demonstrating that our network learns pose- and scale-invariant features that generalize effectively to real-world data.

# Ablations and analyses

**Can pose estimation replace equivariance?** To assess whether an explicit pose estimator can substitute for built-in equivariance, we prepend ConDor [36], a state-of-the-art self-supervised SE(3) pose canonicalizer (no equivalent exists for SIM(3) to our knowledge), to two non-equivariant baselines (PoinTr and AdaPoinTr) on the PCN dataset. As shown in Table 4, ConDor + AdaPoinTr still fails to match the augmentation-based baseline (Table 1), and yields a CD- $\ell_1$  15% higher and an F1 score 3% lower than our SIM(3)-equivariant model; ConDor + PoinTr performs even worse. In contrast, our approach achieves superior accuracy without any explicit pose estimation, demonstrating that architectural equivariance is a more effective design choice.

Table 4: Pose estimation vs. equivariance. Our model ourperforms baselines with pose estimator on PCN.

Method	Transform	CD- $\ell_1 \downarrow$	F1 ↑
ConDor [36] + PoinTr [6]	SE(3)/SE(3)	18.56	0.408
ConDor [36] + AdaPoinTr [7]	SE(3)/SE(3)	9.92	0.692
SIMECO (ours)	I/SIM(3)	<b>8.59</b>	<b>0.714</b>

**How much equivariance is necessary?** Figure 9 plots performance on the PCN Car subset as we progressively swap non-equivariant for SIM(3)-equivariant layers in the encoder/decoder. The non-equivariant baseline [0/0] yields the worst CD- $\ell_1$  and lowest F1. Equipping the encoder with six equivariant layers [6/0] reduces CD- $\ell_1$  and boosts F1. Further introducing four equivariant decoder layers [6/4] yields a slight performance drop, likely due to the overhead from mixing equivariant and non-equivariant modules. Nevertheless, the fully equivariant setup [6/8] attains the best CD- $\ell_1$  and F1, confirming that preserving end-to-end SIM(3) symmetry is essential for optimal shape completion.

Which equivariance group matters most? We ablate training-time equivariance on the PCN Car subset across four operational design domains (ODD): rotation (R), rotation + translation (R + T), rotation + scale (R + S), and full SIM(3) (R + S + T). When directly transferred to KITTI scans (Fig. 10), only the SIM(3) model attains the best Fidelity and MMD. Omitting scale (R + T) or translation (R + S) equivariance increases errors

Table 5: Sensitivity to training-time transforms on PCN Car.

Transform	$\mid \text{CD-}\ell_1 \downarrow$	F1 ↑
SIM(3)/SIM(3)	8.88	0.705
SE(3)/SIM(3)	8.81	0.707
SO(3)/SIM(3)	8.78	0.708
I/SIM(3)	<b>8.76</b>	<b>0.712</b>

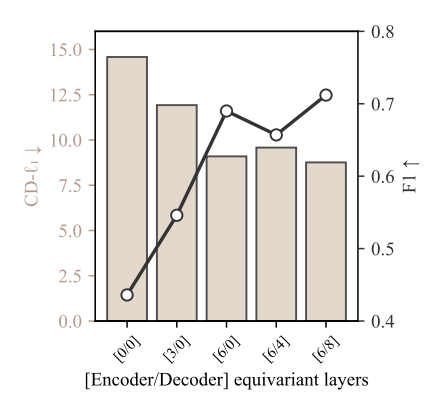
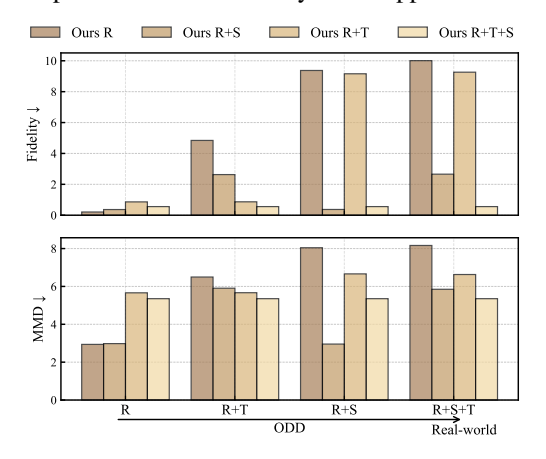


Figure 9: Equivariant layers ablation. On PCN Car, performance increases as non-equivariant layers are progressively replaced with SIM(3)-equivariant ones in the encoder/decoder. The fully equivariant setup delivers the best results.

on both metrics. Notably, the gap between SIM(3) and its subgroups highlights how much more challenging full SIM(3) equivariance is compared to the subgroups. This synthetic-to-real analysis confirms that SIM(3) equivariance is essential for robust, in-the-wild shape completion and further validates our model's advantage over methods limited to SO(3) or SE(3).

Must we canonicalize training data? Real-world data seldom provide objects in a common reference frame, so a practical completion model should tolerate arbitrary pose and scale at training time as well. We therefore *train* our network on the PCN Car subset under four configurations, I, SO(3), SE(3), and SIM(3), and report test performance in Table 5. Across these settings, the average  $CD-\ell_1$  varies by less than 0.15 and the F-score by at most 0.007. The negligible difference demonstrates that our SIM(3)-equivariant architecture learns shape priors that are robust to the transform of training data. Thus, explicit canonicalization of the training data is *not* required.

**Robustness to input noise and point dropout.** Our model, trained exclusively on clean PCN data, degrades gracefully under Gaussian noise up to 0.5% of the object scale, with average CD- $\ell_1$  rising modestly from 8.59 to 9.34 (Fig. 11). It also tolerates substantial point dropout: with a 25% additional dropout rate, F1 remains above 0.69 while CD- $\ell_1$  stays near its drop-free level. These results demonstrate the robustness of our architecture to real-world scans subject to noise and sparsity. We provide additional analyses in Appendix B.



1.00
0.75
0.50
10
0.00
Noise

1.00
0.75
0.50
1.00
0.75
0.00
1.00
0.75
0.75
0.50
1.00
0.75
0.25
0.00
Dropout rate

Figure 10: **Equivariance group ablation.** PCN-trained models evaluated directly on KITTI are endowed with equivariance to rotation (R), translation (T), and scale (S). Each added symmetry group improves performance, with the full SIM(3) model performing best in real-world ODD.

Figure 11: **Robustness to noise and dropout.** Shaded regions show category-wise min-max. Trained solely on clean PCN data, our model remains robust under increasing Gaussian noise and up to 25% additional point dropout.

### 5 Conclusion

We identified SIM(3) equivariance as essential for tackling the persistent pose and scale bias in shape completion and achieving robust generalization. To this end, we introduced the first shape completion architecture composed of inherently SIM(3)-equivariant modules, which effectively disentangle intrinsic geometry from extrinsic transforms. Under a strict, unbiased evaluation protocol that removes all alignment cues, our method sets a new state of the art both on synthetic benchmarks and in direct transfer to unconstrained real scans. These results confirm architectural SIM(3) equivariance as a principled remedy for truly generalizable shape completion. While our current implementation is limited to single-shape completion, extending this framework to multi-object and large-scale scene modeling opens compelling avenues for future work.

# Acknowledgment

This work was supported by TUM Georg Nemetschek Institute under the AI4TWINNING project. We thank Burak Bekci for sharing pretrained ESCAPE weights, Miaowen Dong for helpful discussions, and anonymous reviewers for their constructive comments.

# A Reproducibility

The code repository and demo are publicly accessible via the project page<sup>1</sup>. Detailed instructions for setup and running the code are described in the repository's README.md file.

# **B** Additional Analysis

# **B.1** Input normalization

Table 6 compares two common scale normalization schemes: per-scan bounding-box extents and the global category maximum. Both schemes are consistently applied at training and testing. We observe that the non-equivariant AdaPoinTr [7] is sensitive to the choice and performs better with bounding-box normalization, which we adopt for all competing methods in Sec. 4.2. Our model outperforms AdaPoinTr by a substantial margin, with only marginal improvements when ground-truth extents are available.

Table 6: **Effect of input scale normalization.** "B. box" scales each scan by its bounding box extent, while "max" uses the category's global maximum extent.

Method	Source	Extent	CD− $\ell_1$ ↓	F1 ↑
AdaPoinTr [7]	Input	B. box	9.97	0.629
AdaPoinTr [7]	Input	Max	12.46	0.557
SIMECO (ours)	Input	B. box	8.88	0.705
SIMECO (ours)	GT	B. box	8.76	0.712

#### **B.2** VN-SPD constraint

Imposing the VN-SPD constraint [34] on linear weights yields a more principled optimization than centering-based VN networks, since the center is learned rather than fixed. We validate this with an ablation that replaces VN-SPD with standard VN layers plus centering and normalization on partial inputs. As shown in Table 7, our full model clearly outperforms the centering variant.

Table 7: **Effect of VN-SPD constraint** [34]. The constraint yields a more principled optimization than the centering-based variant.

Method	Transform   Airpl.	Cab.	Car	Chair	Lamp	Sofa	Table	Wat.	CD- $\ell_1 \downarrow$	F1 ↑
AdaPoinTr [7]	SIM(3)/SIM(3)   6.46	12.17	10.51	10.29	7.59	12.26	8.90	8.14	9.54	0.661
SIMECO (centered)	I/SIM(3)   6.10	11.77	10.24	10.05	7.50	12.16	8.57	8.10	9.31	0.673
SIMECO (ours)	I/SIM(3)   6.02	10.75	9.27	9.25	6.66	11.16	7.82	7.77	8.59	0.714

#### **B.3** Computational efficiency

With a batch size of 40, SIMECO trains at about 1 hour per epoch on two NVIDIA A40 GPUs. Fig. 12 reports training losses and validation metrics of SIMECO and AdaPoinTr [7]. SIMECO converges much faster in terms of epochs. AdaPoinTr needs about 140 epochs to reduce  $CD-\ell_1$  below 10, whereas our model does so in only 50 epochs.

Table 8 reports the per-scan latency on PCN. Our model processes a scan in 76 ms end-to-end, about twice as fast as the next-quickest equivariant competitor, ESCAPE [10] (148 ms), and more than twice as fast as EquivPCN [13] (172 ms) and SCARP [15] (172 ms). ESCAPE and SCARP spend extra time in post-processing alignment steps, which inflate total latency beyond the raw inference cost. AdaPoinTr remains faster at 16 ms but achieves this speed without any built-in equivariance. Overall, our method offers the best combination of speed and high-level SIM(3) symmetry preservation.

To isolate the effect of built-in SIM(3) equivariance from model capacity, we compare methods under a similar parameter budget on PCN (Table 9). When scaled to a comparable parameter count, AdaPoinTr improves over its smaller variant yet still trails our model by 0.34 in CD- $\ell_1$ , suggesting that the advantage of equivariance persists after controlling for parameter count.

<sup>1</sup>https://sime-completion.github.io

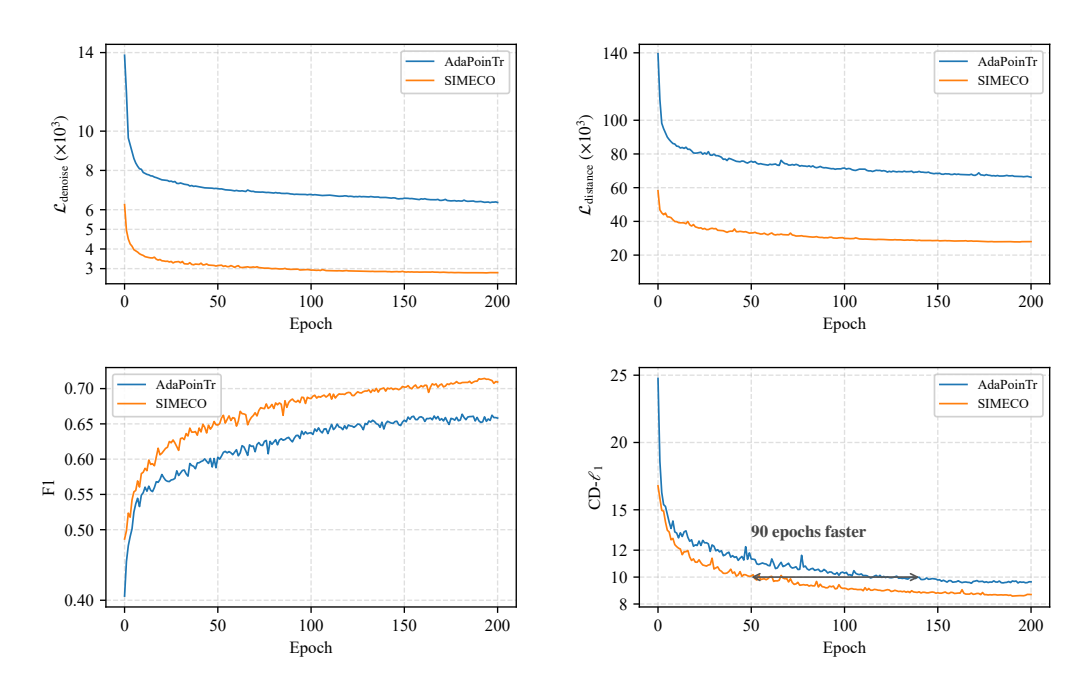


Figure 12: Training losses and validation metrics. Our model converges faster than the baseline.

Table 8: **Average per-scan latency on PCN.** "Inference" denotes the network forward time, measured on an NVIDIA A40 GPU; "Total" adds any post-processing overhead.

Method	Eii	Latency (ms)			
Method	Equivariance	Inference	Total		
AdaPoinTr [7]	I	16.4	16.4		
EquivPCN [13]	SO(3)	171.6	171.6		
SCARP [15]	SE(3)	159.2	172.0		
ESCAPE [10]	SE(3)	18.1	148.4		
SIMECO (ours)	SIM(3)	76.4	76.4		

Table 9: PCN results by parameter count. "#Param. (M)" is the number of parameters (millions).

Method	Transform	#Param. (M)	CD- $\ell_1 \downarrow$	F1 ↑
AdaPoinTr [7]	SIM(3)/SIM(3)	32.49	9.54	0.661
AdaPoinTr [7]	SIM(3)/SIM(3)	57.12	8.93	0.693
SIMECO (ours)	I/SIM(3)	56.96	8.59	0.714

#### **B.4** Performance on thin structures

To evaluate performance on shapes with pronounced thin structures, we compute a local PCA-based anisotropy score:  $L = \frac{\sigma_1 - \sigma_2}{\sigma_1}$  on each point's k-nearest neighbors (k = 30), where  $\sigma_1 \geq \sigma_2 \geq \sigma_3$  are the singular values of the local covariance matrix. A high L indicates a spindly, edge-like neighborhood. We then select shapes in which more than 0.5% of points satisfy L > 0.8, yielding 50 thin-structure cases out of 1200 total. Quantitatively, on this subset, our method achieves an average CD- $\ell 1$  of 6.83, compared to 8.59 over the entire test set, demonstrating even better overall performance on such samples with thin structures. Moreover, qualitative examples such as chair and table legs in Fig. 5 and Fig. 7 further confirm that our method preserves fine details effectively.

#### **B.5** Limitations

Despite its strengths, our approach has several limitations:

- 1. Pose- and scale-dependent features. By construction, we remove any dependence on absolute pose or scale. While this makes the model robust to arbitrary similarity transforms, it can also discard helpful cues when objects always appear in a canonical frame. For instance, a chair back with no visible legs might be mistaken for a sofa because the two shapes coincide under a similarity transform (see Fig. 13). Nevertheless, in realistic settings our method consistently outperforms non-equivariant baselines.
- 2. **Symmetries across partial observations.** The equivariance property in our framework is defined with respect to a single partial scan. For different partial observations of the same object, initialization variability cannot be fully eliminated, thus cross-view symmetries cannot be explicitly enforced and must be learned implicitly from data.
- 3. **Articulated complex scenes.** Our method excels at completing shapes under arbitrary similarity transforms, but it does not explicitly account for independently moving sub-parts (*e.g.*, human joints, robotic arms, or scenes with multiple objects). Incorporating category-specific shape priors or allowing multiple local transforms would be natural extensions to address these more complex scenarios.
- 4. Computational overhead. Vector-valued features and fully equivariant modules incur substantial computation by a factor of three compared to scalar-valued layers. As a result, runtime latency is higher than that of non-equivariant baselines (see Table 8), which may limit real-time or resource-constrained deployments.

#### B.6 Failure cases

Fig. 13 shows two failure cases that rarely occurred in our experiments. Ambiguous partial geometry can entice the network to produce a completion that is plausible yet incorrect. Severe sparsity or noise may disrupt the transform restoration and cause the completed shape to drift from the input frame.



Figure 13: **Failure cases.** Top: ambiguous partial scans leave the network unsure how to complete the shape. Bottom: poor input quality disrupts the transform restoration module and yields misalignment.

# C Proof of SIM(3) Equivariance

In this section, for convenience, we represent 3D vectors as row vectors and stack them into matrices. Specifically, let  $\mathbf{V} \in \mathbb{R}^{D \times 3}$  denote a vector feature, where  $\mathbf{V}[d] \in \mathbb{R}^3$  is its d-th channel, and collect M such features in the set  $\mathcal{V} = \{\mathbf{V}_i\}_{i=1}^M$ . Broadcast vectors  $(e.g., \mathbf{1}_D = [1, 1, \dots, 1]^\top \in \mathbb{R}^{D \times 1})$  are column vectors.

# C.1 Definitions

**Definition 1** (Group invariance). A mapping f is G-invariant (e.g., SIM(3)-invariant) if it satisfies  $f(g \cdot \mathbf{x}) = f(\mathbf{x})$  for all  $g \in G$  and admissible inputs  $\mathbf{x}$ .

**Definition 2** (Group equivariance). A mapping f is G-equivariant (e.g., SIM(3)-equivariant) if it satisfies  $f(g \cdot \mathbf{x}) = g \cdot f(\mathbf{x})$  for all  $g \in G$  and admissible inputs  $\mathbf{x}$ .

#### C.2 SIM(3)-equivariant vector neurons

We assume the input is transformed by an arbitrary  $g = (s, R, t) \in SIM(3)$ , acting on each 3D vector in the VN architecture [32] and the associated matrix as follows:

$$g \cdot \mathbf{V}[d] = sR\mathbf{V}[d] + t, \qquad g \cdot \mathbf{V} = s\mathbf{V}R + \mathbf{1}_D t, \qquad s \in \mathbb{R}^+, \ R \in SO(3), \ t \in \mathbb{R}^3.$$
 (10)

VN-Linear. The VN-Linear layer is defined as a linear transformation shared across the three columns of V:

$$VN-Linear(\mathbf{V}) = \mathbf{W}\mathbf{V}, \quad \mathbf{W} \in \mathbb{R}^{D' \times D}.$$
(11)

For translation equivariance, we constrain each row of the weight matrix W to sum to one [34]:

$$\sum_{i=1}^{D} w_{ij} = 1, \quad w_{ij} \in \mathbf{W} \quad \forall i \in \{1, \dots, D'\}, \quad \Longleftrightarrow \quad \mathbf{W} \mathbf{1}_{D} = \mathbf{1}_{D'}.$$
 (12)

**Proposition 1.** VN-Linear( $\cdot$ ) is SIM(3)-equivariant.

*Proof.* For all  $g \in SIM(3)$ ,

$$VN-Linear(g \cdot V) = W(sVR + \mathbf{1}_D t)$$
(13)

$$= s\mathbf{W}\mathbf{V}R + \mathbf{W}\,\mathbf{1}_D\,t \tag{14}$$

$$= s(\mathbf{W}\mathbf{V})R + \mathbf{1}_{D'}t \tag{15}$$

$$= s \operatorname{VN-Linear}(\mathbf{V})R + \mathbf{1}_{D'} t \tag{16}$$

$$= g \cdot \text{VN-Linear}(\mathbf{V}). \tag{17}$$

**VN-ReLU.** The VN-ReLU layer is constructed via three VN-Linear layers that produce a feature **F**, a direction **B**, and an origin **O**, followed by centering with respect to **O**:

$$(\mathbf{F}, \mathbf{B}, \mathbf{O}) \coloneqq \text{VN-Linear}(\mathbf{V}), \quad \mathbf{F}_{\mathbf{O}} = \mathbf{F} - \mathbf{O}, \quad \mathbf{B}_{\mathbf{O}} = \mathbf{B} - \mathbf{O}.$$
 (18)

The nonlinearity removes the negative projection of  $F_O$  onto the normal  $B_O$  of the plane through O:

$$VN-ReLU(\mathbf{V}) = \begin{cases} \mathbf{O} + \mathbf{F_O} & \text{if } \langle \mathbf{F_O}, \mathbf{B_O} \rangle_F \ge 0 \\ \mathbf{O} + \mathbf{F_O} - \left\langle \mathbf{F_O}, \frac{\mathbf{B_O}}{\|\mathbf{B_O}\|_2} \right\rangle_F \frac{\mathbf{B_O}}{\|\mathbf{B_O}\|_2} & \text{o.w.} \end{cases}$$

$$= \begin{cases} \mathbf{F} & \text{if } \langle \mathbf{F_O}, \mathbf{B_O} \rangle_F \ge 0 \\ \mathbf{F} - \langle \mathbf{F_O}, \mathbf{B_O} \rangle_F \frac{\mathbf{B_O}}{\|\mathbf{B_O}\|_2^2} & \text{o.w.} \end{cases} . \tag{19}$$

**Proposition 2.** VN-ReLU( $\cdot$ ) is SIM(3)-equivaria

*Proof.* For all  $g \in SIM(3)$ ,

$$VN-ReLU(g \cdot \mathbf{V}) \stackrel{(*)}{=} \begin{cases} g \cdot \mathbf{F} & \text{if } \langle s\mathbf{F_O}R, s\mathbf{B_O}R \rangle_F \ge 0 \\ s\mathbf{F}R + \mathbf{1}_D t - \langle s\mathbf{F_O}R, s\mathbf{B_O}R \rangle_F \frac{s\mathbf{B_O}R}{\|s\mathbf{B_O}R\|_2^2} & \text{o.w.} \end{cases}$$

$$\stackrel{(**)}{=} \begin{cases} g \cdot \mathbf{F} & \text{if } s^2 \langle \mathbf{F_O}, \mathbf{B_O} \rangle_F \ge 0 \\ s\mathbf{F}R + \mathbf{1}_D t - s^2 \langle \mathbf{F_O}, \mathbf{B_O} \rangle_F \frac{s\mathbf{B_O}R}{s^2 \|\mathbf{B_O}\|_2^2} & \text{o.w.} \end{cases}$$

$$(20)$$

$$\stackrel{(**)}{=} \begin{cases} g \cdot \mathbf{F} & \text{if } s^2 \langle \mathbf{F_O}, \mathbf{B_O} \rangle_F \ge 0 \\ s \mathbf{F} R + \mathbf{1}_D t - s^2 \langle \mathbf{F_O}, \mathbf{B_O} \rangle_F \frac{s \mathbf{B_O} R}{s^2 \|\mathbf{B_O}\|_2^2} & \text{o.w.} \end{cases}$$
(21)

$$= \begin{cases} g \cdot \mathbf{F} & \text{if } \langle \mathbf{F_O}, \mathbf{B_O} \rangle_F \ge 0 \\ s\mathbf{F}R + \mathbf{1}_D t - s \langle \mathbf{F_O}, \mathbf{B_O} \rangle_F \frac{\mathbf{B_O}}{\|\mathbf{B_O}\|_2^2} R & \text{o.w.} \end{cases}$$
(22)

$$=\begin{cases} g \cdot \mathbf{F} & \text{if } \langle \mathbf{F}_{\mathbf{O}}, \, \mathbf{B}_{\mathbf{O}} \rangle_{F} \geq 0 \\ s \left( \mathbf{F} - \langle \mathbf{F}_{\mathbf{O}}, \, \mathbf{B}_{\mathbf{O}} \rangle_{F} \frac{\mathbf{B}_{\mathbf{O}}}{||\mathbf{B}_{\mathbf{O}}||^{2}} \right) R + \mathbf{1}_{D} t & \text{o.w.} \end{cases}$$
(23)

$$=\begin{cases}g \cdot \mathbf{F} & \text{if } \langle \mathbf{F_O}, \mathbf{B_O} \rangle_F \geq 0\\ s(\mathbf{F} - \langle \mathbf{F_O}, \mathbf{B_O} \rangle_F \frac{\mathbf{B_O}}{\|\mathbf{B_O}\|_2^2})R + \mathbf{1}_D t & \text{o.w.}\end{cases}$$

$$=\begin{cases}g \cdot \mathbf{F} & \text{if } \langle \mathbf{F_O}, \mathbf{B_O} \rangle_F \geq 0\\ g \cdot (\mathbf{F} - \langle \mathbf{F_O}, \mathbf{B_O} \rangle_F \frac{\mathbf{B_O}}{\|\mathbf{B_O}\|_2^2}) & \text{o.w.}\end{cases}$$
(23)

$$= g \cdot \text{VN-ReLU}(\mathbf{V}). \tag{25}$$

Here, (\*) holds because  $\mathbf{F}, \mathbf{B}, \mathbf{O}$  are SIM(3)-equivariant (Prop. 1), and translation cancels in  $\mathbf{F}_{\mathbf{O}}$ and  $\mathbf{B_O}$ . (\*\*) holds as the Frobenius inner product and the  $\ell_2$ -norm are rotation-invariant.

**VN-LeakyReLU.** The VN-LeakyReLU layer is a minor variant of VN-ReLU:

$$VN-LeakyReLU(\mathbf{V}) = \alpha \mathbf{V} + (1 - \alpha) VN-ReLU(\mathbf{V}), \quad \alpha \in (0, 1).$$
 (26)

This operation is trivially SIM(3)-equivariant.

**VN-Max.** The VN-Max layer is defined on a set of vector features  $\mathcal{V}$  by applying two shared VN-Linear layers to each  $V_i \in \mathcal{V}$ , producing a direction  $B_i$  and an origin  $O_i$ , followed by centering with respect to  $O_i$ :

$$(\mathbf{B}_i, \mathbf{O}_i) := \text{VN-Linear}(\mathbf{V}_i), \quad \mathbf{B}_{\mathbf{O},i} = \mathbf{B}_i - \mathbf{O}_i, \quad \mathbf{V}_{\mathbf{O},i} = \mathbf{V}_i - \mathbf{O}_i.$$
 (27)

VN-Max selects, for each channel d, the feature whose centered representation  $V_{O,i}[d]$  is most aligned with its corresponding centered direction  $\mathbf{B}_{\mathbf{O},i}[d]$ :

$$VN\text{-}Max(\mathcal{V})[d] = \mathbf{V}_{i^*}[d], \quad \text{with } i^* = \arg\max_i \langle \mathbf{V}_{\mathbf{O},i}[d], \, \mathbf{B}_{\mathbf{O},i}[d] \rangle_F. \tag{28}$$

**Proposition 3.** VN-Max( $\cdot$ ) is SIM(3)-equivariant.

*Proof.* For all  $g \in SIM(3)$ ,

VN-Max
$$(g \cdot \mathcal{V})[d] = g \cdot \mathbf{V}_{i^*}[d], \text{ with } i^* = \arg \max_i \langle s \mathbf{V}_{\mathbf{O},i}[d] R, s \mathbf{B}_{\mathbf{O},i}[d] R \rangle_F$$
 (29)

$$\stackrel{(*)}{=} \arg \max_{i} s^{2} \langle \mathbf{V}_{\mathbf{O},i}[d], \, \mathbf{B}_{\mathbf{O},i}[d] \rangle_{F} \qquad (30)$$

$$\stackrel{(**)}{=} \arg \max_{i} \langle \mathbf{V}_{\mathbf{O},i}[d], \, \mathbf{B}_{\mathbf{O},i}[d] \rangle_{F} \qquad (31)$$

$$\stackrel{\text{(**)}}{=} \arg \max_{i} \langle \mathbf{V}_{\mathbf{O},i}[d], \, \mathbf{B}_{\mathbf{O},i}[d] \rangle_{F}$$
 (31)

$$VN-Max(g \cdot V)[d] = g \cdot VN-Max(V)[d] \iff VN-Max(g \cdot V) = g \cdot VN-Max(V).$$
 (32)

Here, (\*) holds since the Frobenius inner product is rotation-invariant. (\*\*) holds as the positive scaling factor  $s^2$  preserves the ordering, so the index  $i^*$  remains unchanged.

### C.3 SIM(3)-equivariant Transformer

**Canonicalization.** VN-LayerNorm follows the definition in Sec. 3.2:

$$\mathbf{V}' = \text{VN-LayerNorm}(\mathbf{V}) = \text{layernorm}(\|\mathbf{V} - \bar{\mathbf{V}}\|_2) \cdot \frac{\mathbf{V} - \bar{\mathbf{V}}}{\|\mathbf{V} - \bar{\mathbf{V}}\|_2}, \quad \text{with } \bar{\mathbf{V}} = \frac{1}{D} \sum_{d=1}^{D} \mathbf{V}[d].$$
(33)

**Proposition 4.** VN-LayerNorm $(\cdot)$  is invariant to scaling and translation, and equivariant to rotation.

*Proof.* For all  $g \in SIM(3)$ ,

$$VN-LayerNorm(g \cdot \mathbf{V}) \stackrel{(*)}{=} layernorm \left( \|s\mathbf{V}R - s\bar{\mathbf{V}}R\|_{2} \right) \cdot \frac{(s\mathbf{V}R - s\bar{\mathbf{V}}R)}{\|s\mathbf{V}R - s\bar{\mathbf{V}}R\|_{2}}$$
(34)

$$\stackrel{(**)}{=} \operatorname{layernorm} \left( s \left\| \mathbf{V} - \bar{\mathbf{V}} \right\|_{2} \right) \cdot \frac{\mathbf{V} - \bar{\mathbf{V}}}{\left\| \mathbf{V} - \bar{\mathbf{V}} \right\|_{2}} R \tag{35}$$

$$\stackrel{(***)}{=} \operatorname{layernorm} \left( \left\| \mathbf{V} - \bar{\mathbf{V}} \right\|_{2} \right) \cdot \frac{\mathbf{V} - \bar{\mathbf{V}}}{\left\| \mathbf{V} - \bar{\mathbf{V}} \right\|_{2}} R \tag{36}$$

$$= VN-LayerNorm(\mathbf{V})R. \tag{37}$$

(\*) holds since  $\vec{\mathbf{V}}$  is SIM(3)-equivariant, and translation cancels in differences. (\*\*) holds because the  $\ell_2$ -norm is rotation-invariant. (\*\*\*) holds as layer normalization is invariant to positive scaling. **Shape reasoning.** VN-Attn follows the definition in Sec. 3.2. For self-attention, the input features satisfy  $\mathbf{V}_q' = \mathbf{V}_k' = \mathbf{V}'$ ; for cross-attention,  $\mathbf{V}_q'$  and  $\mathbf{V}_k'$  may differ. These features are the outputs of the canonicalization step, which removes the effects of translation and scale. The query and key are computed via shared VN-Linear layers:

$$\mathbf{Q}_i \coloneqq \text{VN-Linear}(\mathbf{V}'_{q,i}), \quad \mathbf{K}_j \coloneqq \text{VN-Linear}(\mathbf{V}'_{k,j}).$$
 (38)

The attention weight and output are then computed following VN-Transformer [33]:

$$a_{i,j} = \text{VN-Attn}(\mathbf{Q}_i, \mathbf{K}_j) = \text{softmax}_j \left(\frac{1}{\sqrt{3D}} \langle \mathbf{Q}_i, \mathbf{K}_j \rangle_F\right),$$
 (39)

$$\mathbf{Z}_{i} = \sum_{j} a_{i,j} \cdot \text{VN-Linear}(\mathbf{V}'_{k,j}). \tag{40}$$

**Proposition 5.** VN-Attn $(\cdot, \cdot)$  is invariant to rotation, and  $\mathbf{Z}_i$  is equivariant to rotation.

*Proof.* Rotation invariance of VN-Attn $(\cdot, \cdot)$  follows immediately from the fact that the Frobenius inner product is rotation-invariant. Because  $a_{i,j}$  is rotation-invariant and, by Prop. 1, VN-Linear $(\cdot)$  is rotation-equivariant, it follows that  $\mathbf{Z}_i$  is rotation-equivariant.

**Transform restoration.** Transform restoration follows the definition in Sec. 3.2. Given the module input **V** and the attention output **Z**, the restored output is then computed as

$$TR(\mu, \mathbf{V}, \mathbf{Z}) = \mathbf{V} + VN-Linear(\mu \mathbf{Z}), \text{ with } \mu = \mathbb{E}_D \|\mathbb{E}_i(\mathbf{V}_i - \bar{\mathbf{V}}_i)\|_2, \quad \bar{\mathbf{V}}_i = \frac{1}{D} \sum_{d=1}^D \mathbf{V}_i[d].$$
(41)

**Proposition 6.**  $TR(\cdot, \cdot, \cdot)$  can recover SIM(3) equivariance.

*Proof.* For all  $g \in SIM(3)$ 

$$TR(g \cdot (\mu, \mathbf{V}, \mathbf{Z})) \stackrel{(*)}{=} s\mathbf{V}R + \mathbf{1}_D t + VN-Linear(s\mu \mathbf{Z}R)$$
(42)

$$\stackrel{(**)}{=} s\mathbf{V}R + \mathbf{1}_D t + s\mu VN-Linear(\mathbf{Z})R$$
 (43)

$$= s(\mathbf{V} + \mu VN\text{-Linear}(\mathbf{Z}))R + \mathbf{1}_D t \tag{44}$$

$$= g \cdot TR((\mu, \mathbf{V}, \mathbf{Z})) \tag{45}$$

Here, (\*) holds because the attention output **Z** encodes only the effect of rotation (Prop. 4 and Prop. 5). The scalar  $\mu$  scales with s, as translation is eliminated by differencing, and the  $\ell_2$ -norm is rotation-invariant. Hence,

$$\mathbb{E}_D \| \mathbb{E}_i (g \cdot (\mathbf{V}_i - \bar{\mathbf{V}}_i)) \|_2 = s \cdot \mathbb{E}_D \| \mathbb{E}_i (\mathbf{V}_i - \bar{\mathbf{V}}_i) \|_2. \tag{46}$$

#### C.4 Other modules

**VN-DGCNN.** VN-DGCNN performs edge feature extraction and aggregation across layers [7, 32]:

$$\mathbf{V}_{i}^{l+1} = \text{VN-Max}_{j \in \mathcal{N}_{i}} \left( \text{VNLA} \left( (\mathbf{V}_{j}^{l} + \bar{\mathbf{V}}^{l} - \mathbf{V}_{i}^{l}) \oplus \mathbf{V}_{i}^{l} \right) \right), \quad \text{with} \quad \bar{\mathbf{V}}^{l} = \frac{1}{M} \sum_{i=1}^{M} \mathbf{V}_{i}^{l}. \tag{47}$$

where  $\mathcal{N}_i$  is the KNN neighborhood of point i, and  $\oplus$  denotes feature concatenation. VNLA $(\cdot)$  applies VN-Linear $(\cdot)$  followed by VN-LeakyReLU $(\cdot)$ . Because each edge feature  $(\mathbf{V}_j^l + \bar{\mathbf{V}}^l - \mathbf{V}_i^l) \oplus \mathbf{V}_i^l$  preserves SIM(3) equivariance, and both VNLA $(\cdot)$  and VN-Max $(\cdot)$  are SIM(3)-equivariant (Prop. 1, Prop. 2, and Prop. 3), each layer output remains equivariant. By layer-wise induction, the entire VN-DGCNN is SIM(3)-equivariant. We initialize all vector features  $\mathbf{V}$  with the 3D coordinates of the input points.

**Query generator.** The query generator produces a fused query set  $\mathbf{Q} = [\mathbf{Q}_I, \mathbf{Q}_G]$  [7], where  $\mathbf{Q}_I$  is sampled from the partial input and  $\mathbf{Q}_G = \text{VN-Linear}(\text{VN-Max}(\mathcal{V}))$ , with  $\mathcal{V}$  denoting the output of the final encoder layer.  $\mathbf{Q}$  is SIM(3)-equivariant, as  $\mathbf{Q}_I$  follows the transformed input, and  $\mathbf{Q}_G$  inherits equivariance from the encoder through SIM(3)-equivariant operations (Prop. 1 and Prop. 3).

**Reconstruction head.** The reconstruction head produces the final output point set  $\hat{y}$  as:

$$\hat{\mathbf{y}} = \text{VN-Linear}(\mathbf{V} - \bar{\mathbf{V}}) + \mathbf{Q}, \text{ with } \bar{\mathbf{V}} = \frac{1}{D} \sum_{d=1}^{D} \mathbf{V}[d].$$
 (48)

where V is the decoder output.  $\hat{y}$  is SIM(3)-equivariant, as centering V prevents translation accumulation from V and Q, with both the VN-Linear( $\cdot$ ) and Q preserving equivariance (Prop. 1).

# C.5 Summary and approximate equivariance bound

The entire network architecture is SIM(3)-equivariant by construction, since it is built exclusively from the above-mentioned SIM(3)-equivariant modules. To stabilize training, we follow the practice of Assaad *et al.* [33] and introduce a small norm-controlled bias to VN-Linear layers. Although this modification introduces a minor deviation from exact equivariance, its effect in each layer is bounded by a constant  $\epsilon_l$ , and remains insignificant across layers as proved in VN-Transformer [33]. As a result, the overall network is effectively  $\epsilon_{1...L}$ -approximately equivariant.

# **D** Implementation Details

SIMECO is implemented in PyTorch and optimized using the Adam optimizer with an initial learning rate of  $10^{-4}$ , a weight decay of  $5 \times 10^{-4}$ , and a learning-rate decay factor of 0.9 every 15 epochs. We adopt the same architectural depth and hyperparameters as AdaPoinTr [7]. The models, including baselines, were trained for 200 epochs on two NVIDIA A40 GPUs. All other completion methods [6, 7, 8, 10, 13, 15, 54, 64] were used with their default settings.

#### **E** More Visualizations

Fig. 14 expands the PCN comparison with more methods. Fig. 15 presents further qualitative results on KITTI and OmniObject3D scans. Fig. 16 shows how the methods respond to controlled pose and scale perturbations.

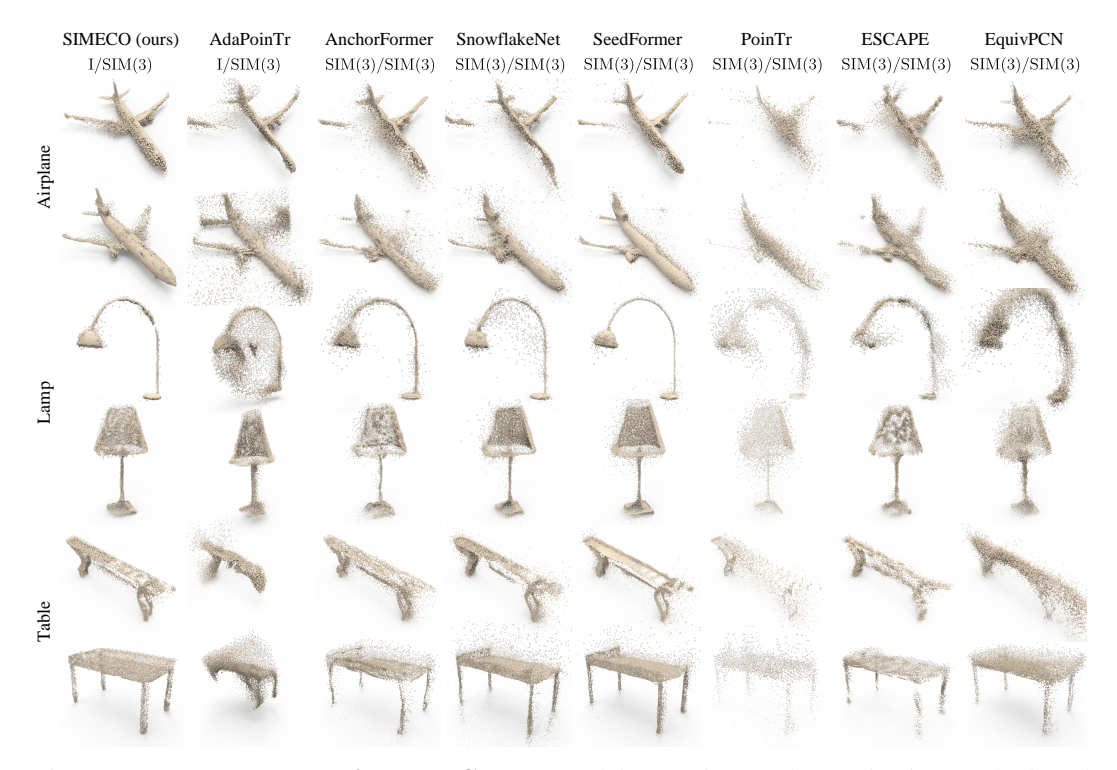


Figure 14: **Extended comparison on PCN.** Our model outperforms other equivariant methods and non-equivariant baselines trained with SIM(3) augmentation. Complements Fig. 5.

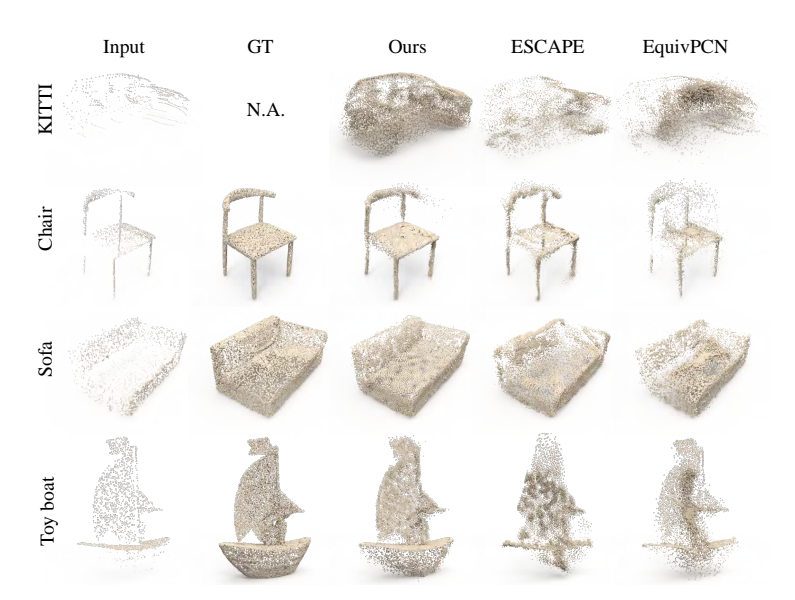


Figure 15: Extended cross-domain comparison. Our PCN-trained model completes driving (KITTI) and indoor (OmniObject3D) scans more accurately than other methods with SIM(3) augmentation. Complements Fig. 7.

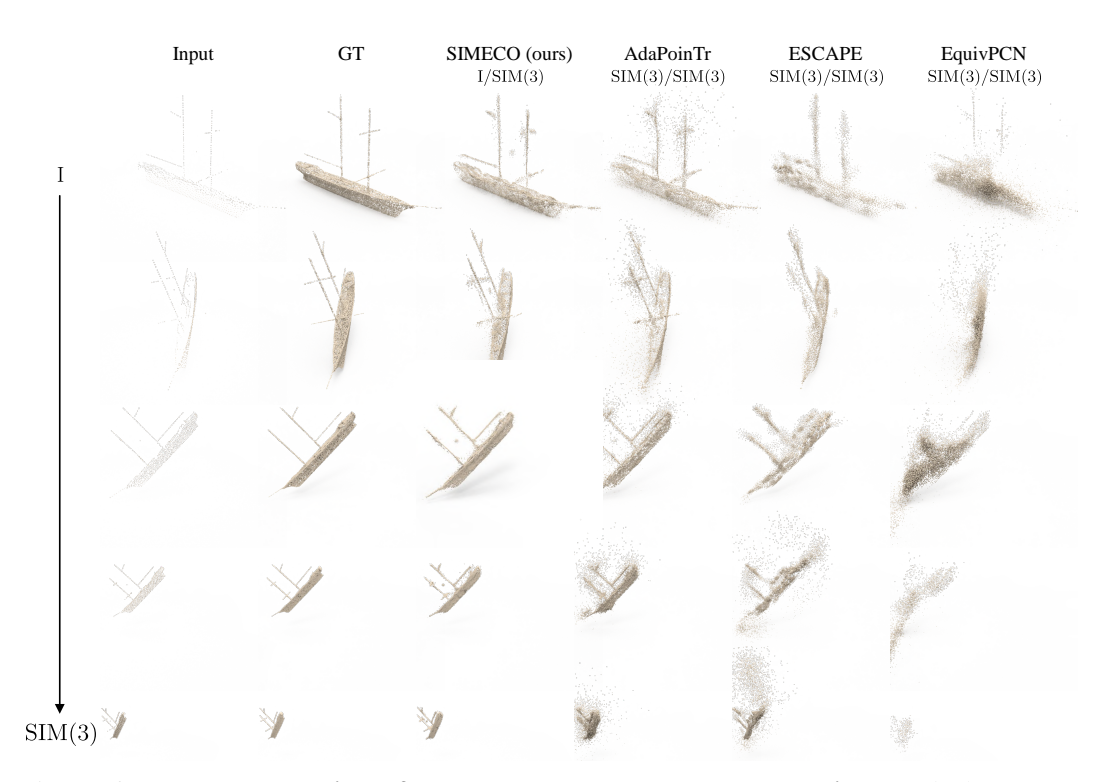


Figure 16: Extended comparison of robustness to pose and scale perturbations. Under larger pose and scale changes, our  $\mathrm{SIM}(3)$ -equivariant model maintains completion quality, whereas competing methods degrade. Complements Fig. 6.

#### References

- [1] Ramesh Ashok Tabib, Dikshit Hegde, Tejas Anvekar, and Uma Mudenagudi. DeFi: detection and filling of holes in point clouds towards restoration of digitized cultural heritage models. In *Proceedings of the IEEE/CVF International conference on computer vision*, pages 1603–1612, 2023.
- [2] Theodore Tsesmelis, Luca Palmieri, Marina Khoroshiltseva, Adeela Islam, Gur Elkin, Ofir I Shahar, Gianluca Scarpellini, Stefano Fiorini, Yaniv Ohayon, Nadav Alali, et al. Re-assembling the past: The RePAIR dataset and benchmark for real world 2D and 3D puzzle solving. *Advances in Neural Information Processing Systems*, 37:30076–30105, 2024.
- [3] Chaoda Zheng, Feng Wang, Naiyan Wang, Shuguang Cui, and Zhen Li. Towards flexible 3D perception: Object-centric occupancy completion augments 3D object detection. In *Advances in Neural Information Processing Systems*, 2024.
- [4] Jacob Varley, Chad DeChant, Adam Richardson, Joaquín Ruales, and Peter Allen. Shape completion enabled robotic grasping. In *IEEE/RSJ international conference on intelligent robots and systems*, pages 2442–2447. IEEE, 2017.
- [5] Haozhe Xie, Hongxun Yao, Shangchen Zhou, Jiageng Mao, Shengping Zhang, and Wenxiu Sun. GRNet: Gridding residual network for dense point cloud completion. In *European conference on computer vision*, pages 365–381. Springer, 2020.
- [6] Xumin Yu, Yongming Rao, Ziyi Wang, Zuyan Liu, Jiwen Lu, and Jie Zhou. PoinTr: Diverse point cloud completion with geometry-aware transformers. In *Proceedings of the IEEE/CVF international conference on computer vision*, pages 12498–12507, 2021.
- [7] Xumin Yu, Yongming Rao, Ziyi Wang, Jiwen Lu, and Jie Zhou. AdaPoinTr: Diverse point cloud completion with adaptive geometry-aware transformers. *IEEE Transactions on Pattern Analysis & Machine Intelligence*, 45(12):14114–14130, December 2023.
- [8] Zhikai Chen, Fuchen Long, Zhaofan Qiu, Ting Yao, Wengang Zhou, Jiebo Luo, and Tao Mei. AnchorFormer: Point cloud completion from discriminative nodes. In *Proceedings of the IEEE/CVF conference on computer vision and pattern recognition*, pages 13581–13590, 2023.
- [9] Wu Yushuang, Yan Zizheng, Chen Ce, Wei Lai, Li Xiao, Li Guanbin, Li Yihao, Cui Shuguang, and Han Xiaoguang. SCoDA: Domain adaptive shape completion for real scans. In *The IEEE/CVF Computer Vision and Pattern Recognition Conference*, 2023.
- [10] Burak Bekci, Nassir Navab, Federico Tombari, and Mahdi Saleh. ESCAPE: Equivariant shape completion via anchor point encoding. In *Proceedings of the IEEE/CVF Conference on Computer Vision and Pattern Recognition*, 2025.
- [11] Taco S Cohen, Mario Geiger, Jonas Köhler, and Max Welling. Spherical CNNs. In *International Conference on Learning Representations*, 2018.
- [12] Nathaniel Thomas, Tess Smidt, Steven Kearnes, Lusann Yang, Li Li, Kai Kohlhoff, and Patrick Riley. Tensor field networks: Rotation-and translation-equivariant neural networks for 3D point clouds. *arXiv preprint arXiv:1802.08219*, 2018.
- [13] Hang Wu and Yubin Miao. SO(3) rotation equivariant point cloud completion using attention-based vector neurons. In 2022 International Conference on 3D Vision, pages 280–290. IEEE, 2022.
- [14] Driton Salihu, Adam Misik, Yuankai Wu, Constantin Patsch, Fabian Seguel, and Eckehard Steinbach. DeepSPF: Spherical SO(3)-equivariant patches for Scan-to-CAD estimation. In *International Conference on Learning Representations*, 2024.
- [15] Bipasha Sen, Aditya Agarwal, Gaurav Singh, Srinath Sridhar, Madhava Krishna, et al. SCARP: 3D shape completion in arbitrary poses for improved grasping. In 2023 IEEE International Conference on Robotics and Automation, pages 3838–3845. IEEE, 2023.

- [16] Hanmo Xu, Qingyao Shuai, and Xuejin Chen. PCLC-Net: Point cloud completion in arbitrary poses with learnable canonical space. In *Computer Graphics Forum*, volume 43, page e15217. Wiley Online Library, 2024.
- [17] Taco Cohen and Max Welling. Group equivariant convolutional networks. In *International conference on machine learning*, pages 2990–2999. PMLR, 2016.
- [18] Carlos Esteves, Christine Allen-Blanchette, Ameesh Makadia, and Kostas Daniilidis. Learning SO(3) equivariant representations with spherical CNNs. In *European conference on computer vision*, pages 52–68, 2018.
- [19] Jimmy Aronsson. Homogeneous vector bundles and G-equivariant convolutional neural networks. Sampling Theory, Signal Processing, and Data Analysis, 20(2):10, 2022.
- [20] Taco Cohen, Maurice Weiler, Berkay Kicanaoglu, and Max Welling. Gauge equivariant convolutional networks and the icosahedral CNN. In *International conference on Machine learning*, pages 1321–1330. PMLR, 2019.
- [21] Taco S Cohen, Mario Geiger, and Maurice Weiler. A general theory of equivariant cnns on homogeneous spaces. *Advances in neural information processing systems*, 32, 2019.
- [22] Risi Kondor and Shubhendu Trivedi. On the generalization of equivariance and convolution in neural networks to the action of compact groups. In *International conference on machine learning*, pages 2747–2755. PMLR, 2018.
- [23] Maurice Weiler, Patrick Forré, Erik Verlinde, and Max Welling. Coordinate independent convolutional networks–isometry and gauge equivariant convolutions on riemannian manifolds. *arXiv* preprint arXiv:2106.06020, 2021.
- [24] Yinshuang Xu, Jiahui Lei, Edgar Dobriban, and Kostas Daniilidis. Unified fourier-based kernel and nonlinearity design for equivariant networks on homogeneous spaces. In *International Conference on Machine Learning*, pages 24596–24614. PMLR, 2022.
- [25] Wen Shen, Binbin Zhang, Shikun Huang, Zhihua Wei, and Quanshi Zhang. 3D-rotation-equivariant quaternion neural networks. In *European Conference on Computer Vision*, pages 531–547, 2020.
- [26] Sharvaree Vadgama, Mohammad Mohaiminul Islam, Domas Buracas, Christian Shewmake, Artem Moskalev, and Erik Bekkers. Probing equivariance and symmetry breaking in convolutional networks. *arXiv preprint arXiv:2501.01999*, 2025.
- [27] David R Wessels, David M Knigge, Samuele Papa, Riccardo Valperga, Sharvaree Vadgama, Efstratios Gavves, and Erik J Bekkers. Grounding continuous representations in geometry: Equivariant neural fields. *arXiv preprint arXiv:2406.05753*, 2024.
- [28] Haiwei Chen, Shichen Liu, Weikai Chen, Hao Li, and Randall Hill. Equivariant point network for 3D point cloud analysis. In *Proceedings of the IEEE/CVF conference on computer vision and pattern recognition*, pages 14514–14523, 2021.
- [29] Minghan Zhu, Maani Ghaffari, William A Clark, and Huei Peng. E2PN: Efficient SE(3)-equivariant point network. In *Proceedings of the IEEE/CVF Conference on Computer Vision and Pattern Recognition*, pages 1223–1232, 2023.
- [30] Jaein Kim, Hee Bin Yoo, Dong-Sig Han, Yeon-Ji Song, and Byoung-Tak Zhang. Continuous SO(3) equivariant convolution for 3D point cloud analysis. In *European Conference on Computer Vision*, pages 59–75. Springer, 2024.
- [31] Fabian Fuchs, Daniel Worrall, Volker Fischer, and Max Welling. SE(3)-Transformers: 3D roto-translation equivariant attention networks. *Advances in neural information processing systems*, 33:1970–1981, 2020.
- [32] Congyue Deng, Or Litany, Yueqi Duan, Adrien Poulenard, Andrea Tagliasacchi, and Leonidas J Guibas. Vector neurons: A general framework for SO(3)-equivariant networks. In *Proceedings of the IEEE/CVF International Conference on Computer Vision*, pages 12200–12209, 2021.

- [33] Serge Assaad, Carlton Downey, Rami Al-Rfou, Nigamaa Nayakanti, and Ben Sapp. VN-Transformer: Rotation-equivariant attention for vector neurons. *arXiv preprint* arXiv:2206.04176, 2022.
- [34] Oren Katzir, Dani Lischinski, and Daniel Cohen-Or. Shape-pose disentanglement using SE(3)equivariant vector neurons. In *European Conference on Computer Vision*, pages 468–484. Springer, 2022.
- [35] Xiaolong Li, Yijia Weng, Li Yi, Leonidas J Guibas, A Abbott, Shuran Song, and He Wang. Leveraging SE(3) equivariance for self-supervised category-level object pose estimation from point clouds. *Advances in neural information processing systems*, 34:15370–15381, 2021.
- [36] Rahul Sajnani, Adrien Poulenard, Jivitesh Jain, Radhika Dua, Leonidas J Guibas, and Srinath Sridhar. ConDor: Self-supervised canonicalization of 3D pose for partial shapes. In *Proceedings* of the IEEE/CVF Conference on Computer Vision and Pattern Recognition, pages 16969–16979, 2022.
- [37] Haoran Pan, Jun Zhou, Yuanpeng Liu, Xuequan Lu, Weiming Wang, Xuefeng Yan, and Mingqiang Wei. SO(3)-Pose: SO(3)-equivariance learning for 6D object pose estimation. In *Computer Graphics Forum*, volume 41, pages 371–381. Wiley Online Library, 2022.
- [38] Cheng-Wei Lin, Tung-I Chen, Hsin-Ying Lee, Wen-Chin Chen, and Winston H Hsu. Coarse-to-fine point cloud registration with SE(3)-equivariant representations. In 2023 IEEE international conference on robotics and automation, pages 2833–2840. IEEE, 2023.
- [39] Chien Erh Lin, Minghan Zhu, and Maani Ghaffari. SE3ET: SE(3)-equivariant transformer for low-overlap point cloud registration. *IEEE Robotics and Automation Letters*, 2024.
- [40] Jingyun Yang, Zi-ang Cao, Congyue Deng, Rika Antonova, Shuran Song, and Jeannette Bohg. EquiBot: Sim(3)-equivariant diffusion policy for generalizable and data efficient learning. *arXiv* preprint arXiv:2407.01479, 2024.
- [41] Jingyun Yang, Congyue Deng, Jimmy Wu, Rika Antonova, Leonidas Guibas, and Jeannette Bohg. EquivAct: SIM(3)-equivariant visuomotor policies beyond rigid object manipulation. In 2024 IEEE international conference on robotics and automation, pages 9249–9255. IEEE, 2024.
- [42] Evangelos Chatzipantazis, Stefanos Pertigkiozoglou, Edgar Dobriban, and Kostas Daniilidis. SE(3)-equivariant attention networks for shape reconstruction in function space. *arXiv* preprint *arXiv*:2204.02394, 2022.
- [43] Yinshuang Xu, Jiahui Lei, and Kostas Daniilidis. Equivariant light field convolution and transformer. *arXiv preprint arXiv:2212.14871*, 2022.
- [44] Yinshuang Xu, Dian Chen, Katherine Liu, Sergey Zakharov, Rareş Ambruş, Kostas Daniilidis, and Vitor Guizilini. SE(3) equivariant ray embeddings for implicit multi-view depth estimation. *Advances in Neural Information Processing Systems*, 37:13627–13659, 2024.
- [45] Hong-Xing Yu, Jiajun Wu, and Li Yi. Rotationally equivariant 3D object detection. In *Proceedings of the IEEE/CVF conference on computer vision and pattern recognition*, pages 1456–1464, 2022.
- [46] Jiahui Lei, Congyue Deng, Karl Schmeckpeper, Leonidas Guibas, and Kostas Daniilidis. EFEM: Equivariant neural field expectation maximization for 3D object segmentation without scene supervision. In *Proceedings of the IEEE/CVF Conference on Computer Vision and Pattern Recognition*, pages 4902–4912, 2023.
- [47] Angela Dai, Charles Ruizhongtai Qi, and Matthias Nießner. Shape completion using 3D-encoder-predictor CNNs and shape synthesis. In *Proceedings of the IEEE conference on computer vision and pattern recognition*, pages 5868–5877, 2017.
- [48] Xiaoguang Han, Zhen Li, Haibin Huang, Evangelos Kalogerakis, and Yizhou Yu. High-resolution shape completion using deep neural networks for global structure and local geometry inference. In *Proceedings of the IEEE international conference on computer vision*, pages 85–93, 2017.

- [49] Zhirong Wu, Shuran Song, Aditya Khosla, Fisher Yu, Linguang Zhang, Xiaoou Tang, and Jianxiong Xiao. 3D ShapeNets: A deep representation for volumetric shapes. In *Proceedings of the IEEE conference on computer vision and pattern recognition*, pages 1912–1920, 2015.
- [50] Charles R Qi, Hao Su, Kaichun Mo, and Leonidas J Guibas. PointNet: Deep learning on point sets for 3D classification and segmentation. In *Proceedings of the IEEE conference on computer vision and pattern recognition*, pages 652–660, 2017.
- [51] Wentao Yuan, Tejas Khot, David Held, Christoph Mertz, and Martial Hebert. PCN: Point completion network. In 2018 international conference on 3D vision (3DV), pages 728–737. IEEE, 2018.
- [52] Yaoqing Yang, Chen Feng, Yiru Shen, and Dong Tian. FoldingNet: Point cloud auto-encoder via deep grid deformation. In *Proceedings of the IEEE conference on computer vision and pattern recognition*, pages 206–215, 2018.
- [53] Ashish Vaswani, Noam Shazeer, Niki Parmar, Jakob Uszkoreit, Llion Jones, Aidan N Gomez, Łukasz Kaiser, and Illia Polosukhin. Attention is all you need. Advances in neural information processing systems, 30, 2017.
- [54] Haoran Zhou, Yun Cao, Wenqing Chu, Junwei Zhu, Tong Lu, Ying Tai, and Chengjie Wang. SeedFormer: Patch seeds based point cloud completion with upsample transformer. In *European conference on computer vision*, pages 416–432. Springer, 2022.
- [55] Sangho Lee, Hayun Lee, and Dongkun Shin. ProxyFormer: Nyström-based linear transformer with trainable proxy tokens. In *Proceedings of the AAAI Conference on Artificial Intelligence*, volume 38, pages 13418–13426, 2024.
- [56] Pingping Cai, Deja Scott, Xiaoguang Li, and Song Wang. Orthogonal dictionary guided shape completion network for point cloud. In *Proceedings of the AAAI conference on Artificial Intelligence*, pages 864–872, 2024.
- [57] Zhaiyu Chen, Yuqing Wang, Liangliang Nan, and Xiao Xiang Zhu. Parametric point cloud completion for polygonal surface reconstruction. In *Proceedings of the IEEE/CVF Conference on Computer Vision and Pattern Recognition*, 2025.
- [58] Weixiao Gao, Ravi Peters, and Jantien Stoter. Building-PCC: Building point cloud completion benchmarks. *ISPRS Annals of the Photogrammetry, Remote Sensing and Spatial Information Sciences*, pages 179–186, 2024.
- [59] Jimmy Lei Ba, Jamie Ryan Kiros, and Geoffrey E Hinton. Layer normalization. *arXiv preprint arXiv:1607.06450*, 2016.
- [60] Yunlu Chen, Basura Fernando, Hakan Bilen, Matthias Nießner, and Efstratios Gavves. 3D equivariant graph implicit functions. In *European Conference on Computer Vision*, pages 485–502. Springer, 2022.
- [61] Angel X Chang, Thomas Funkhouser, Leonidas Guibas, Pat Hanrahan, Qixing Huang, Zimo Li, Silvio Savarese, Manolis Savva, Shuran Song, Hao Su, et al. ShapeNet: An information-rich 3D model repository. *arXiv preprint arXiv:1512.03012*, 2015.
- [62] Andreas Geiger, Philip Lenz, Christoph Stiller, and Raquel Urtasun. Vision meets robotics: The KITTI dataset. *International Journal of Robotics Research*, 2013.
- [63] Tong Wu, Jiarui Zhang, Xiao Fu, Yuxin Wang, Liang Pan Jiawei Ren, Wayne Wu, Lei Yang, Jiaqi Wang, Chen Qian, Dahua Lin, and Ziwei Liu. OmniObject3D: Large-vocabulary 3D object dataset for realistic perception, reconstruction and generation. In *IEEE/CVF Conference on Computer Vision and Pattern Recognition*, 2023.
- [64] Peng Xiang, Xin Wen, Yu-Shen Liu, Yan-Pei Cao, Pengfei Wan, Wen Zheng, and Zhizhong Han. SnowflakeNet: Point cloud completion by snowflake point deconvolution with skip-transformer. In *Proceedings of the IEEE/CVF international conference on computer vision*, pages 5499–5509, 2021.

# **NeurIPS Paper Checklist**

#### 1. Claims

Question: Do the main claims made in the abstract and introduction accurately reflect the paper's contributions and scope?

Answer: [Yes]

Justification: Our contributions and scope are summarized in Sec. 1, and supported by Sec. 3, Sec. 4, and the Appendix with theoretical and experimental evidence.

#### Guidelines:

- The answer NA means that the abstract and introduction do not include the claims made in the paper.
- The abstract and/or introduction should clearly state the claims made, including the contributions made in the paper and important assumptions and limitations. A No or NA answer to this question will not be perceived well by the reviewers.
- The claims made should match theoretical and experimental results, and reflect how much the results can be expected to generalize to other settings.
- It is fine to include aspirational goals as motivation as long as it is clear that these goals
  are not attained by the paper.

#### 2. Limitations

Question: Does the paper discuss the limitations of the work performed by the authors?

Answer: [Yes]

Justification: We briefly acknowledge application-level constraints in Sec. 5 and provide a comprehensive discussion of limitations and computational scalability in the Appendix.

#### Guidelines:

- The answer NA means that the paper has no limitation while the answer No means that the paper has limitations, but those are not discussed in the paper.
- The authors are encouraged to create a separate "Limitations" section in their paper.
- The paper should point out any strong assumptions and how robust the results are to violations of these assumptions (e.g., independence assumptions, noiseless settings, model well-specification, asymptotic approximations only holding locally). The authors should reflect on how these assumptions might be violated in practice and what the implications would be.
- The authors should reflect on the scope of the claims made, e.g., if the approach was only tested on a few datasets or with a few runs. In general, empirical results often depend on implicit assumptions, which should be articulated.
- The authors should reflect on the factors that influence the performance of the approach. For example, a facial recognition algorithm may perform poorly when image resolution is low or images are taken in low lighting. Or a speech-to-text system might not be used reliably to provide closed captions for online lectures because it fails to handle technical jargon.
- The authors should discuss the computational efficiency of the proposed algorithms and how they scale with dataset size.
- If applicable, the authors should discuss possible limitations of their approach to address problems of privacy and fairness.
- While the authors might fear that complete honesty about limitations might be used by reviewers as grounds for rejection, a worse outcome might be that reviewers discover limitations that aren't acknowledged in the paper. The authors should use their best judgment and recognize that individual actions in favor of transparency play an important role in developing norms that preserve the integrity of the community. Reviewers will be specifically instructed to not penalize honesty concerning limitations.

#### 3. Theory assumptions and proofs

Question: For each theoretical result, does the paper provide the full set of assumptions and a complete (and correct) proof?

Answer: [Yes]

Justification: Each theorem in Sec. 3, including the equivariance results, states all assumptions and refers to formal proofs in the Appendix.

#### Guidelines:

- The answer NA means that the paper does not include theoretical results.
- All the theorems, formulas, and proofs in the paper should be numbered and crossreferenced.
- All assumptions should be clearly stated or referenced in the statement of any theorems.
- The proofs can either appear in the main paper or the supplemental material, but if they appear in the supplemental material, the authors are encouraged to provide a short proof sketch to provide intuition.
- Inversely, any informal proof provided in the core of the paper should be complemented by formal proofs provided in appendix or supplemental material.
- Theorems and Lemmas that the proof relies upon should be properly referenced.

# 4. Experimental result reproducibility

Question: Does the paper fully disclose all the information needed to reproduce the main experimental results of the paper to the extent that it affects the main claims and/or conclusions of the paper (regardless of whether the code and data are provided or not)?

Answer: [Yes]

Justification: All experimental protocols are detailed in Sec. 4.1 and the Appendix using public datasets, and our code is provided for full reproduction.

#### Guidelines:

- The answer NA means that the paper does not include experiments.
- If the paper includes experiments, a No answer to this question will not be perceived well by the reviewers: Making the paper reproducible is important, regardless of whether the code and data are provided or not.
- If the contribution is a dataset and/or model, the authors should describe the steps taken to make their results reproducible or verifiable.
- Depending on the contribution, reproducibility can be accomplished in various ways. For example, if the contribution is a novel architecture, describing the architecture fully might suffice, or if the contribution is a specific model and empirical evaluation, it may be necessary to either make it possible for others to replicate the model with the same dataset, or provide access to the model. In general, releasing code and data is often one good way to accomplish this, but reproducibility can also be provided via detailed instructions for how to replicate the results, access to a hosted model (e.g., in the case of a large language model), releasing of a model checkpoint, or other means that are appropriate to the research performed.
- While NeurIPS does not require releasing code, the conference does require all submissions to provide some reasonable avenue for reproducibility, which may depend on the nature of the contribution. For example
  - (a) If the contribution is primarily a new algorithm, the paper should make it clear how to reproduce that algorithm.
- (b) If the contribution is primarily a new model architecture, the paper should describe the architecture clearly and fully.
- (c) If the contribution is a new model (e.g., a large language model), then there should either be a way to access this model for reproducing the results or a way to reproduce the model (e.g., with an open-source dataset or instructions for how to construct the dataset).
- (d) We recognize that reproducibility may be tricky in some cases, in which case authors are welcome to describe the particular way they provide for reproducibility. In the case of closed-source models, it may be that access to the model is limited in some way (e.g., to registered users), but it should be possible for other researchers to have some path to reproducing or verifying the results.

# 5. Open access to data and code

Question: Does the paper provide open access to the data and code, with sufficient instructions to faithfully reproduce the main experimental results, as described in supplemental material?

Answer: [Yes],

Justification: All datasets are publicly available. Our supplemental material includes code with instructions, and we will publicly release the repository upon acceptance.

#### Guidelines:

- The answer NA means that paper does not include experiments requiring code.
- Please see the NeurIPS code and data submission guidelines (https://nips.cc/public/guides/CodeSubmissionPolicy) for more details.
- While we encourage the release of code and data, we understand that this might not be possible, so "No" is an acceptable answer. Papers cannot be rejected simply for not including code, unless this is central to the contribution (e.g., for a new open-source benchmark).
- The instructions should contain the exact command and environment needed to run to reproduce the results. See the NeurIPS code and data submission guidelines (https://nips.cc/public/guides/CodeSubmissionPolicy) for more details.
- The authors should provide instructions on data access and preparation, including how to access the raw data, preprocessed data, intermediate data, and generated data, etc.
- The authors should provide scripts to reproduce all experimental results for the new proposed method and baselines. If only a subset of experiments are reproducible, they should state which ones are omitted from the script and why.
- At submission time, to preserve anonymity, the authors should release anonymized versions (if applicable).
- Providing as much information as possible in supplemental material (appended to the paper) is recommended, but including URLs to data and code is permitted.

# 6. Experimental setting/details

Question: Does the paper specify all the training and test details (e.g., data splits, hyperparameters, how they were chosen, type of optimizer, etc.) necessary to understand the results?

Answer: [Yes]

Justification: Sec. 3.3, Sec. 4.1, and the Appendix detail training, evaluation, and code.

#### Guidelines:

- The answer NA means that the paper does not include experiments.
- The experimental setting should be presented in the core of the paper to a level of detail that is necessary to appreciate the results and make sense of them.
- The full details can be provided either with the code, in appendix, or as supplemental material.

#### 7. Experiment statistical significance

Question: Does the paper report error bars suitably and correctly defined or other appropriate information about the statistical significance of the experiments?

Answer: [No]

Justification: Results are based on single runs over fixed splits, and error bars are omitted due to computational constraints. However, Sec. 4 demonstrates consistent, statistically significant performance across multiple datasets.

- The answer NA means that the paper does not include experiments.
- The authors should answer "Yes" if the results are accompanied by error bars, confidence intervals, or statistical significance tests, at least for the experiments that support the main claims of the paper.

- The factors of variability that the error bars are capturing should be clearly stated (for example, train/test split, initialization, random drawing of some parameter, or overall run with given experimental conditions).
- The method for calculating the error bars should be explained (closed form formula, call to a library function, bootstrap, etc.)
- The assumptions made should be given (e.g., Normally distributed errors).
- It should be clear whether the error bar is the standard deviation or the standard error
  of the mean.
- It is OK to report 1-sigma error bars, but one should state it. The authors should preferably report a 2-sigma error bar than state that they have a 96% CI, if the hypothesis of Normality of errors is not verified.
- For asymmetric distributions, the authors should be careful not to show in tables or figures symmetric error bars that would yield results that are out of range (e.g. negative error rates).
- If error bars are reported in tables or plots, The authors should explain in the text how they were calculated and reference the corresponding figures or tables in the text.

#### 8. Experiments compute resources

Question: For each experiment, does the paper provide sufficient information on the computer resources (type of compute workers, memory, time of execution) needed to reproduce the experiments?

Answer: [Yes]

Justification: We detail the hardware specification and runtimes in the Appendix.

#### Guidelines:

- The answer NA means that the paper does not include experiments.
- The paper should indicate the type of compute workers CPU or GPU, internal cluster, or cloud provider, including relevant memory and storage.
- The paper should provide the amount of compute required for each of the individual experimental runs as well as estimate the total compute.
- The paper should disclose whether the full research project required more compute than the experiments reported in the paper (e.g., preliminary or failed experiments that didn't make it into the paper).

#### 9. Code of ethics

Question: Does the research conducted in the paper conform, in every respect, with the NeurIPS Code of Ethics https://neurips.cc/public/EthicsGuidelines?

Answer: [Yes]

Justification: Our research fully complies with the NeurIPS Code of Ethics.

#### Guidelines:

- The answer NA means that the authors have not reviewed the NeurIPS Code of Ethics.
- If the authors answer No, they should explain the special circumstances that require a deviation from the Code of Ethics.
- The authors should make sure to preserve anonymity (e.g., if there is a special consideration due to laws or regulations in their jurisdiction).

#### 10. Broader impacts

Question: Does the paper discuss both potential positive societal impacts and negative societal impacts of the work performed?

Answer: [No]

Justification: Our academic work presents foundational methods evaluated on standard public benchmarks with no explicit negative societal impacts.

# Guidelines:

• The answer NA means that there is no societal impact of the work performed.

- If the authors answer NA or No, they should explain why their work has no societal impact or why the paper does not address societal impact.
- Examples of negative societal impacts include potential malicious or unintended uses (e.g., disinformation, generating fake profiles, surveillance), fairness considerations (e.g., deployment of technologies that could make decisions that unfairly impact specific groups), privacy considerations, and security considerations.
- The conference expects that many papers will be foundational research and not tied to particular applications, let alone deployments. However, if there is a direct path to any negative applications, the authors should point it out. For example, it is legitimate to point out that an improvement in the quality of generative models could be used to generate deepfakes for disinformation. On the other hand, it is not needed to point out that a generic algorithm for optimizing neural networks could enable people to train models that generate Deepfakes faster.
- The authors should consider possible harms that could arise when the technology is being used as intended and functioning correctly, harms that could arise when the technology is being used as intended but gives incorrect results, and harms following from (intentional or unintentional) misuse of the technology.
- If there are negative societal impacts, the authors could also discuss possible mitigation strategies (e.g., gated release of models, providing defenses in addition to attacks, mechanisms for monitoring misuse, mechanisms to monitor how a system learns from feedback over time, improving the efficiency and accessibility of ML).

#### 11. Safeguards

Question: Does the paper describe safeguards that have been put in place for responsible release of data or models that have a high risk for misuse (e.g., pretrained language models, image generators, or scraped datasets)?

Answer: [NA]

Justification: We do not foresee any explicit risk for misuse of this work.

#### Guidelines:

- The answer NA means that the paper poses no such risks.
- Released models that have a high risk for misuse or dual-use should be released with
  necessary safeguards to allow for controlled use of the model, for example by requiring
  that users adhere to usage guidelines or restrictions to access the model or implementing
  safety filters.
- Datasets that have been scraped from the Internet could pose safety risks. The authors should describe how they avoided releasing unsafe images.
- We recognize that providing effective safeguards is challenging, and many papers do not require this, but we encourage authors to take this into account and make a best faith effort.

#### 12. Licenses for existing assets

Question: Are the creators or original owners of assets (e.g., code, data, models), used in the paper, properly credited and are the license and terms of use explicitly mentioned and properly respected?

Answer: [Yes]

Justification: We have credited them appropriately.

- The answer NA means that the paper does not use existing assets.
- The authors should cite the original paper that produced the code package or dataset.
- The authors should state which version of the asset is used and, if possible, include a URL.
- The name of the license (e.g., CC-BY 4.0) should be included for each asset.
- For scraped data from a particular source (e.g., website), the copyright and terms of service of that source should be provided.

- If assets are released, the license, copyright information, and terms of use in the
  package should be provided. For popular datasets, paperswithcode.com/datasets
  has curated licenses for some datasets. Their licensing guide can help determine the
  license of a dataset.
- For existing datasets that are re-packaged, both the original license and the license of the derived asset (if it has changed) should be provided.
- If this information is not available online, the authors are encouraged to reach out to the asset's creators.

#### 13. New assets

Question: Are new assets introduced in the paper well documented and is the documentation provided alongside the assets?

Answer: [Yes]

Justification: Source code is provided in the Supplementary Material with full documentation and will be publicly released for reproducibility.

#### Guidelines:

- The answer NA means that the paper does not release new assets.
- Researchers should communicate the details of the dataset/code/model as part of their submissions via structured templates. This includes details about training, license, limitations, etc.
- The paper should discuss whether and how consent was obtained from people whose asset is used.
- At submission time, remember to anonymize your assets (if applicable). You can either create an anonymized URL or include an anonymized zip file.

# 14. Crowdsourcing and research with human subjects

Question: For crowdsourcing experiments and research with human subjects, does the paper include the full text of instructions given to participants and screenshots, if applicable, as well as details about compensation (if any)?

Answer: [NA]

Justification: This work involves no crowdsourcing or human-subject research.

# Guidelines:

- The answer NA means that the paper does not involve crowdsourcing nor research with human subjects.
- Including this information in the supplemental material is fine, but if the main contribution of the paper involves human subjects, then as much detail as possible should be included in the main paper.
- According to the NeurIPS Code of Ethics, workers involved in data collection, curation, or other labor should be paid at least the minimum wage in the country of the data collector.

# 15. Institutional review board (IRB) approvals or equivalent for research with human subjects

Question: Does the paper describe potential risks incurred by study participants, whether such risks were disclosed to the subjects, and whether Institutional Review Board (IRB) approvals (or an equivalent approval/review based on the requirements of your country or institution) were obtained?

Answer: [NA]

Justification: This work involves no human-subject research.

- The answer NA means that the paper does not involve crowdsourcing nor research with human subjects.
- Depending on the country in which research is conducted, IRB approval (or equivalent) may be required for any human subjects research. If you obtained IRB approval, you should clearly state this in the paper.

- We recognize that the procedures for this may vary significantly between institutions and locations, and we expect authors to adhere to the NeurIPS Code of Ethics and the guidelines for their institution.
- For initial submissions, do not include any information that would break anonymity (if applicable), such as the institution conducting the review.

# 16. Declaration of LLM usage

Question: Does the paper describe the usage of LLMs if it is an important, original, or non-standard component of the core methods in this research? Note that if the LLM is used only for writing, editing, or formatting purposes and does not impact the core methodology, scientific rigorousness, or originality of the research, declaration is not required.

Answer: [NA]

Justification: The core method development does not involve LLMs.

- The answer NA means that the core method development in this research does not involve LLMs as any important, original, or non-standard components.
- Please refer to our LLM policy (https://neurips.cc/Conferences/2025/LLM) for what should or should not be described.